PCCP

ROYAL SOCIETY OF CHEMISTRY

PAPER

View Article Online
View Journal | View Issue

Cite this: *Phys. Chem. Chem. Phys.*, 2024, **26**, 9432

Weak hydrogen bonding to halogens and chirality communication in propanols: Raman and microwave spectroscopy benchmark theory†‡

Beppo Hartwig, [a] Melanie Schnell, [bc] Martin A. Suhm [a] and Daniel A. Obenchain *[a]

Constitutional and conformational isomers of bromopropanol are vibrationally and rotationally characterised with parallels drawn to the structural chlorine analogues. A previous microwave spectroscopic study of the chloropropanols is re-examined and all systems are explored by Raman jet spectroscopy. For bromine, the entire nuclear quadrupole coupling tensors are accurately determined and compared to their chlorine counterparts. Tensor asymmetry parameters are determined and linked with the hydrogen bond strength as indicated by the downshift of the OH-stretching frequency. The spectroscopic constants derived from the observed transitions are used as benchmarks for a large variety of electronic structure methods followed by harmonic and anharmonic rovibrational treatments. The CCSD(T) electronic structure calculations provide the best performance, in particular once anharmonic and relativistic corrections are applied or implied. Standard DFT approaches vary substantially with respect to their systematic error cancellation across the investigated species, and cost-effective compromises for the different observables are proposed.

Received 10th October 2023,
Accepted 22nd February 2024

DOI: 10.1039/d3cp04911f

rsc.li/pccp

1 Introduction

Asymmetrically substituted and thus chiral carbon atoms have an influence on the preferred chirality of their molecular or supramolecular environment.[1,2] If the environment is conformationally flexible, the chiral influence translates into conformational preferences. This chirality induction phenomenon[3] is systematically exploited in asymmetric synthesis,[4] and it is accessible to different kinds of gas-phase spectroscopies.[3,5–7] It is therefore of major interest to better understand the through-bond (covalent) and through-space (non-covalent) influence of a chiral centre on its immediate neighbourhood in simple model systems. From the perspective of the three-point model of chirality recognition,[8] particularly suitable molecular model systems could be those which embed the chiral centre into its environment by one chemical bond, one hydrogen bond, and by an additional weak repulsive or dispersive interaction.

One of the simplest intramolecular sources of chirality induction is a carbon atom with an H, a CH_3, a halogen X and a CH_2OH group attached. The latter has two conformational degrees of freedom, the OH internal rotation around the CO bond and the CO bond internal rotation relative to the rest. Both torsional degrees of freedom can adopt their axial handedness to the chiral centre in the resulting 2-X-propan-1-ols. For X = Cl, the chiral alcohol has played an important role in the discovery of chirality recognition by another chiral species in the gas phase.[9] A constitutional isomer of this historically important model alcohol is obtained when the X and OH groups are exchanged. This changes the CO bond internal rotation into a CX bond internal rotation relative to the molecular frame, but otherwise the possibility of chirality induction remains the same in the resulting 1-X-propan-2-ols. The two isomeric halogenated propanols are thus convenient study partners to work out differences and similarities.[10] They

[a] *Institut für Physikalische Chemie, Tammannstrasse 6, 37077 Göttingen, Germany. E-mail: daniel.obenchain@uni-goettingen.de*
[b] *Deutsches Elektronen-Synchrotron DESY, Notkestr. 85, 22607 Hamburg, Germany*
[c] *Institute of Physical Chemistry, Christian-Albrechts-Universität zu Kiel, Max-Eyth-Straße 1, 24118 Kiel, Germany*

† Electronic supplementary information (ESI) available: The standard PDF document in the ESI contains relative electronic and zero-point corrected energies, vibrational assignments, experimental conditions, experimental rotational constants, and example inputs and details with regards to the computation of the distortion constants. See DOI: **https://doi.org/10.1039/d3cp04911f**

‡ The experimental details as well as their associated raw vibrational spectra can be found here (**https://doi.org/10.25625/EJVBHD**). The relative electronic and zero point corrected energies, vibrational assignments, predicted/experimental rotational constants, rotational line lists, and CCSD(T) xyz-files are published as a separate dataset (**https://doi.org/10.25625/CTG8TD**). The raw cavity microwave data are provided in a separate dataset (**https://doi.org/10.25625/S5PEGU**). The latter two data sets can be found together in a dataverse (**https://data.goettingen-research-online.de/dataverse/esi_mw_bromo_chloropropanols**).

offer subtle variants of the requested combination of a chemical bond, a hydrogen bond, and weaker interactions from the chiral centre to its molecular surrounding. Another helpful tuning parameter is the halogen X, which will be varied from Cl to Br in the present study.

Two aspects make these twin pairs of halogenated propanols particularly interesting: the possibility of a bridging interaction between the OH group and the X atom (often called a hydrogen bond despite its steric constraints and resulting weakness) and the nuclear quadrupole moment which comes with stable halogen nuclei if their (due to a strong preference for neutron pairs) half-integer spin exceeds 1/2. The nuclear quadrupole allows to probe the electric field gradient at the halogen nucleus, which is influenced by the hydrogen bond.[10] The bridging hydrogen interaction brings folded conformations down in energy, such that *gauche* ($\approx 60^\circ$) torsional angles in the pentatomic HOCCX arrangement will regularly win over *trans* or *anti* ($\approx 180^\circ$) arrangements.[11,12] More than that, the two *gauche* torsions in the five-membered ring have to be opposite in sign in order to close the hydrogen bridge in such a small model system. This is different from extended chain systems, where the sergeant-and-soldiers effect often induces helical sequences of the same torsional angle sign.[1]

As a result, a binary conformational competition emerges in these highly flexible model propanols. Will an (*R*) configuration at the stereogenic center induce a +− sequence in the two relevant, appropriately ordered torsional angles, or a −+ sequence instead? The opposite will naturally be true for an (*S*) configuration at the asymmetric carbon atom. This binary choice in the leading conformations of X-propanols has been pioneered for X = Cl using microwave spectroscopy.[10] The present work further explores it in a number of ways, always with the intention to benchmark quantum-chemical methods in their ability to predict the chirality induction effects through chemical and hydrogen bonds. It combines microwave with Raman spectroscopy, it extends from the previously studied Cl case to the experimentally more favourable Br homologue (large quadrupole coupling constant), and it tries to find a relationship between hydrogen bond induced shifts and the asymmetry of the nuclear quadrupole coupling tensor.

2 Methodology

2.1 Experimental methods

2.1.1 Raman spectrocopy. To record Raman spectra in dilute supersonic expansions, a sensitive detection scheme (the so called *curry*-jet described in ref. 11 and 13–15) was employed. Briefly, a gas mixture of helium and small amounts of the alcohol (see ESI,† Table S3 for details of the compounds and gases used) is continuously expanded through a slit nozzle. To regulate the concentration of the alcohol, a coolable saturator was used and kept at 275 K and 285 K for the chloropropanols and bromopropanols, respectively. A backing pressure of 0.4 bar (0.6 bar) was used for the chloropropanols (bromopropanols) with He as a carrier gas. A Spectra Physics Millenia 25 eV continuous laser irradiated the expansion orthogonally 1.0 mm downstream from the nozzle with 20 W of 532 nm radiation. Exposure times of 4 min for the scattered radiation have been used in all cases, and the Raman spectra have a resolution of 1 cm^{-1}. The raw experimental spectra have been made available in ref. 16. A more detailed overview of the expansion conditions can be found in the ESI.† The Raman spectra in the 3560–3700 cm^{-1} region, including a discussion of potential impurities,[17–22] can also be found in the ESI.†

2.1.2 Microwave spectrocopy. In the 2–8 GHz frequency range the COMPACT setup of the Schnell group was used, which has previously been described in detail in ref. 23 and 24. Here, chirped-pulse Fourier transform microwave (CP-FTMW) spectroscopy was applied, which allows for the fast acquisition of broadband microwave spectra. Using a pulse rate of 8 Hz for the expansion, during each gas pulse, the expansion was irradiated eight times with 4 μs long microwave chirps in the 2–8 GHz range. Each chirp is amplified with a 300 W amplifier. To broadcast the chirped pulse a horn antenna is used. Opposite to the broadcasting antenna, another antenna collects the free induction decay (FID) for 40 μs, hence, an overall repetition rate of 64 Hz can be achieved, resulting in a frequency resolution of 25 kHz. The samples (see ESI,† Table S3 for details of the compounds and gases used) were kept at room temperature and 325 K for 2-bromopropan-1-ol and 1-bromopropan-2-ol, respectively, with a backing pressure of 2.4 bar in both cases. The samples were held in the reservoir section of a modified General Valve Series 9 solenoid valve, directly at the valve orifice. Ne was used as a carrier gas.

To improve the quality of the fits with respect to the off-diagonal components of the nuclear quadrupole coupling tensor, further measurements were made on the Q-CUMBER spectrometer in Göttingen. This includes additional measurements for 1-bromopropan-2-ol, 1-chloropropan-2-ol, and 2-chloropropan-1-ol with backing pressures around 1.4 bar with Ne as a carrier gas. The sample is introduced 4 cm before a General Valve Series 9 solenoid valve, but no heating of the sample was needed on the cavity instrument. This spectrometer was formerly developed at the University of Kiel[25] and is based on the original Fabry–Perot cavity designed by Balle and Flygare[26] and a coaxial mirror-expansion arrangement and runs on the FTMW++ software developed in Hannover.[27]

The I^r representation ($z \mapsto a$, $x \mapsto b$, and $y \mapsto c$) and Watson's *S* reduction have been used throughout using H. M. Pickett's SPFIT program[28] to fit the rotational spectra. In case of the bromopropanols, the nuclear spin-rotation interaction constants C_{aa}, C_{bb}, and C_{cc} are fitted, which help to lower the experimental uncertainties of the nuclear quadrupole coupling constants (NQCCs), especially for the off-diagonal elements. C_{ii} arises from the coupling of the magnetic moment of the nucleus with the magnetic field arising from the rotation of the molecule and largely depends on the nuclear magnetic dipole moments of the chlorine (μ_{Cl}) and bromine (μ_{Br}) atoms. Given that μ_{Cl} is significantly smaller than μ_{Br}, C_{aa}, C_{bb} and C_{cc} could not be determined for the chloropropanols. Instead of fitting C_{ii} for the bromopropanols, testing was done with the

Table 1 Summary of relevant constants in the Watson *S* reduction for the microwave spectra. Constants is abbreviated as const., and NQC stands for nuclear quadrupole coupling

Constant	Explanation
A, B, C	Rotational const.
D_J, D_K, D_{JK}	Diagonal quartic centrifugal distortion const.
d_1, d_2	Off-diagonal quartic centrifugal distortion const.
χ_{aa}, χ_{bb-cc}	Diagonal NQC const.
χ_{ab}, χ_{ac}, χ_{bc}	Off-diagonal NQC const.
χ_J, χ_K	Quartic NQC distortion const.
C_{aa}, C_{bb}, C_{cc}	Nuclear spin-rotation interaction const.

quartic distortion constants of the NQCCs (χ_J and χ_K). However, χ_J and χ_K could either not be well determined and/or did not improve the fit significantly. Hence, fitting χ_J and χ_K was disregarded. Since C_{ii} could not be determined for the chloropropanols, no attempt of fitting χ_J and χ_K was made in that case. A brief overview of all relevant constants is provided in Table 1.

2.2 Computational methods

A large variety of different calculations have been conducted using the ORCA 4.2.1,[29–31] Gaussian 16 (Rev. A.03)[32] and Molpro 2020.2[33–35] program packages. On the density functional theory (DFT) side, functionals of different rungs of the so called Jacob's Ladder have been utilised, ranging from GGAs up to double-hybrid functionals. The lowest level of DFT used in this work comprises the BP86[36–38] and PBE[39] functionals, which utilise the generalized gradient approximation (GGA). By introducing second and higher order derivatives of the electron density, one arrives at the *meta*-GGA rung. From this family, the TPSS[40] functional was used. Moving up the ladder, the hybrid functionals B3LYP[38,41,42] and PBE0[43,44] were employed. These hybrid functionals utilise a constant amount of exact Hartree–Fock (HF) exchange. This can be improved by including a dependence upon the electron–electron distance for the HF exchange. Such range-separated hybrid functionals[45] include the CAM-B3LYP[46] method used in this work. Another approach to improve functionals is to explicitly include parts of the correlation energy from wavefunction methods. A reasonably inexpensive option is second-order Møller–Plesset perturbation theory (MP2).[47] Such methods were first proposed by S. Grimme[48,49] and are referred to as double-hybrid functionals of which his initially proposed B2PLYP functional was used in this work. For all functionals, Grimme's D3 dispersion correction was added in conjunction with Becke–Johnson damping (D3(BJ)).[50,51] Three body terms of the Axilrod–Teller–Muto[52,53] type are included (D3(BJ,abc)) when using the ORCA package. For brevity, the D3 label will be dropped, and its use is always implied for calculations conducted for this work. All methods used are summarised in Table 2.

BP86, PBE, PBE0 and B3LYP calculations have been conducted with the ORCA program package utilising the ma-def2-TZVP (maTZ)[54] basis set, a minimally augmented variant of the def2-TZVP[55] basis set. In a previous study, this basis set proved to be an efficient compromise between accuracy and computational cost.[56] The Grid5 integration grid was used together with the TightOpt geometry optimisation threshold. The optimisation was then followed by an analytical frequency calculation[57] within the double harmonic approximation. Moreover, the RI-J approximation was utilised for BP86 and PBE with the corresponding auxiliary basis set,[58] while for PBE0 and B3LYP no density fitting was used. To compute the Raman activities needed to simulate the vibrational spectra, the procedure outlined in ref. 59 was used.

Table 2 Overview of the different methods used. The type of dispersion correction is given if applicable. The ma-def2-TZVP and aug-cc-pVTZ basis sets have been shortened to maTZ and aTZ, respectively. When Gaussian was used as a program, VPT2 calculations have been conducted. For all other programs, only harmonic frequencies have been computed

Method	Dispersion	Basis set	Program
BP86	D3(BJ,abc)	maTZ	ORCA
PBE	D3(BJ,abc)	maTZ	ORCA
TPSS	D3(BJ)	aTZ	Gaussian
PBE0	D3(BJ,abc)	maTZ	ORCA
PBE0	D3(BJ)	aTZ	Gaussian
B3LYP	D3(BJ,abc)	maTZ	ORCA
B3LYP	D3(BJ)	aTZ	Gaussian
CAM-B3LYP	D3(BJ)	aTZ	Gaussian
B2PLYP	D3(BJ)	aTZ	Gaussian
MP2	—	aTZ	Gaussian
CCSD(T)-F12a	—	VDZ-F12	Molpro

Gaussian was used to conduct TPSS, PBE0, B3LYP, CAM-B3LYP, B2PLYP and MP2 calculations. The SuperFine grid and VeryTight optimisation criteria were used. Following the optimisation, vibrational perturbation theory of second order (VPT2)[60] in Gaussian's efficient implementation[61,62] was applied. The harmonic frequency part is computed analytically. In all cases, the aug-cc-pVTZ[63,64] basis set was used and no density fitting was applied. The VPT2 calculations also yield centrifugal distortion constants (CDCs), and their derivation is described in more detail in the ESI† (Section 5). The computation of the CDCs at the coupled cluster level (harmonic frequency calculation conducted with Molpro) is also elaborated on in the ESI,† with the necessary theory being outlined in ref. 65–67.

Molpro was used for geometry optimisations (analytical gradients)[68,69] and (numerical) harmonic frequency calculations at the CCSD(T)-F12a[70,71] level of theory. The coupled cluster calculations include single (S), double (D) and perturbative triple ((T)) excitations. Additionally, explicit correlation (F12a) was used, in conjunction with the specialised VDZ-F12[72] basis set, to accelerate the basis set convergence. In case of Br, the VDZ-PP-F12[73] basis set, which utilises a (Stuttgart–Köln type ECP10MDF) pseudo potential[74] to describe the core electrons, was used. The mixed VDZ-F12 and VDZ-PP-F12 basis set is referred to as VDZ-F12*. In all cases, density fitting was used with the corresponding auxiliary basis sets.[75–78]

Furthermore, using the CCSD(T) geometries computed with Molpro, CCSD(T) calculations have been conducted with ORCA to compute the electric field gradient (EFG), q_{ij}, at the Cl and Br nuclei. From the EFG, the nuclear quadrupole coupling constants χ_{ij} (NQCC) can be derived, which will be described in more detail in the next paragraph. Since q_{ij} does not only depend on the valence orbitals but also the core orbitals, the specialised aug-cc-pwCVTZ[64,79,80] basis set was used. Moreover, a recent study by Aerts and Brown[81] extensively tested coupled cluster calculations with aug-cc-pVXZ and aug-cc-pwCVXZ (X = D, T, Q, 5) basis sets of which aug-cc-pwCVTZ (shortened to awCTZ) provides a good compromise between accuracy and computational cost. Neither the frozen core approximation nor density fitting was used. Relativistic effects are likely to play a role for Br, while Cl should be largely unaffected as previous studies have shown.[82–84] To this end, relativistic calculations have been conducted using the Douglas–Kroll–Hess of second order (DKH2)[85–87] transformation. For these calculations, the finite nucleus model[88] and picture change effects[89] are included. It should be noted that basis sets adapted specifically for DKH2 calculations may provide better results than the aug-cc-pwCVTZ basis set used here. The use of DKH2 will be indicated by a -D at the end of the method.

χ_{ij} can be computed in the following way:

$$\chi_{ij} = \frac{eQq_{ij}}{h} = eQ\frac{\partial^2 V_{ij}}{\partial x_i \partial x_j}\frac{1}{h} \quad (1)$$

$$\frac{\chi_{ij}}{\mathrm{MHz}} = 235.541 \times \frac{Q}{\mathrm{barn}} \times \frac{q_{ij}}{E_\mathrm{h}/ea_0^2} \quad (2)$$

Here, e is the elementary charge, Q the nuclear quadrupole moment, V_{ij} the electrostatic potential and h Planck's constant. i and j refer to the axes in the inertial reference frame (a, b, c). Eqn (2) shows a direct way to convert the q_{ij} in atomic units ($1E_\mathrm{h}/ea_0{}^2 \approx 9.717 \times 10^{21}$ V m^{-2}) to χ_{ij} in MHz with Q in barn (1 barn $\equiv$ 100 fm^2). The Q ($Q(^{79}\mathrm{Br}) = +0.313(3)$, $Q(^{81}\mathrm{Br}) = +0.262(3)$, $+0.262(3)$, $Q(^{35}\mathrm{Cl}) = -0.817(8)$, and $Q(^{37}\mathrm{Cl}) = -0.0644(7)$) used in this work are based on the recommendations of the International Nuclear Data Committee.[90] For consistency, we do not use the revised Q for Br of Stopkowicz *et al.*[82] In case of calculations conducted with Gaussian, χ_{ij} is directly computed in MHz and the default Q are used instead. We would like to remind the reader that q_{ij} and by extension χ_{ij} tensors are traceless ($\chi_{aa} + \chi_{bb} + \chi_{cc} = 0$ MHz) and symmetric ($\chi_{ab} = \chi_{ba}$, $\chi_{ac} = \chi_{ca}$ and $\chi_{bc} = \chi_{cb}$). Therefore, χ_{aa}, χ_{bb-cc}, χ_{ab}, χ_{ac} and χ_{bc} are sufficient for a full characterisation. Furthermore, as long as the algebraic sign of the product of the off-diagonal elements is kept, different descriptions are equivalent, *e.g.* $\chi_{ab}\chi_{ac}\chi_{bc} = (-\chi_{ab})(-\chi_{ac})\chi_{bc}$.

Example inputs for all calculations can be found in the ESI† (Section 7).

2.3 Nomenclature

In a previous study, Goldstein *et al.*[10] investigated the chloropropanols and used an adapted nomenclature[91] based on the work of Al-Rabaa *et al.*[92] Here, we use a simplified variant with the same descriptors for the two constitutional isomers. As a reference point, the (*R*) enantiomer of the different alcohols is arbitrarily chosen. The *gauche* HO–CC$_\mathrm{X}$ dihedral angle is specified by a lower case g, while an upper case G describes the XC–CO dihedral angle where X corresponds to Br or Cl. A prime (′) added indicates a negative sign of the *gauche* angle. In case of 2-bromopropan-1-ol, gG′ thus refers to a HO–CC$_\mathrm{Br}$ angle of roughly 60° and a BrC–CO angle of about −60°. Within this nomenclature, gG′ conveniently remains the most stable conformer for all studied systems. The different conformers are shown in Fig. 2 for the Br case. The Cl conformers are analogous in structure. gG′ corresponds to g-ga and m-ga conformers and g′G to g′-gg and h-gg in the nomenclature used by Goldstein *et al.*[10]

3 Results

3.1 Predicted chirality induction energetics

Before sequentially presenting the experimental results for bromo- and chloropropanols and discussing theory performance for different observables and spectroscopic constants derived from them, a comparative survey over the predicted energetics for the four pairs of gG′/g′G isomers shall be given, within the harmonic approximation for the zero point vibrational energy. Note that on an absolute scale, the constitutional isomers 1-X-propan-2-ol and 2-X-propan-1-ol are predicted by coupled cluster theory to differ by about 4 kJ mol^{-1} (X = Cl) and 7 kJ mol^{-1} (X = Br) at zero point level, with the secondary alcohols being more stable (see ESI,† for other computational levels). This energy difference between the constitutional isomers shall be disregarded in the present work, which instead focuses on the conformational energy difference between the less stable g′G isomer for an *R*-configured alcohol and its more stable gG′ isomer for each individual bromo- and chloropropanol, *i.e.*, the chirality induction effect of the asymmetric carbon.

Fig. 1 illustrates this energy difference after harmonic zero point energy correction (ΔE_0^h). Comparison between the red (1-ols) and black (2-ols) as well as between the Br (dashed) and Cl (dotted) sequences allows for several observations. BP86/maTZ is an outlier because it inverts (Br) or cancels (Cl) the conformational energy order between 1-ols and 2-ols. For all other employed methods, the chirality induction for 1-ols exceeds that for 2-ols, which is a remarkably consistent result, previously predicted for Cl.[10] Where maTZ and aTZ basis set results are available, the differences are negligible, thus validating the previous use of the much faster maTZ basis set for DFT calculations.[56] The switch from Cl to Br is seen to have a small and systematic attenuation effect on the magnitude of chirality induction in most cases. The two largest exceptions are B2PLYP, where the Cl/Br difference is amplified, and CCSD(T), for which Br shows a particularly small chirality induction for the 2-ol. This can be seen in the energy difference of the far right entry (red) in Fig. 1. One might suspect the use of a Br pseudopotential as an explanation for the latter effect, as it is the only case where MP2 differs significantly from CCSD(T).

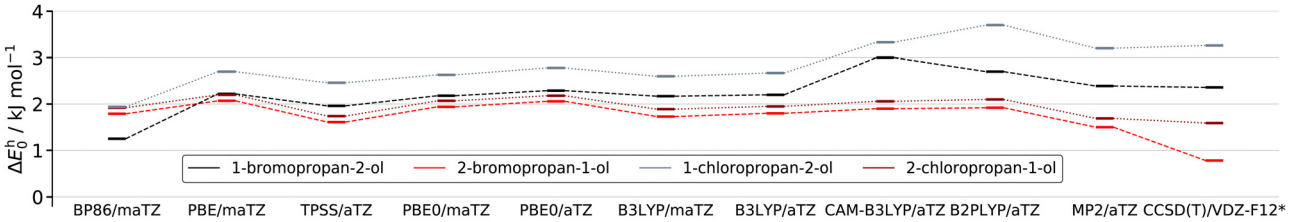

Fig. 1 Overview of the harmonic zero-point corrected g′G energies (ΔE_0^h) relative to the gG′ ground states of 2-bromopropan-1-ol (red), 2-chloropropan-1-ol (dark red), 1-bromopropan-2-ol (black), and 1-chloropropan-2-ol (grey) at different levels of theory. For ease of identification, energy levels for the bromopropanols are connected by dashed lines while the chloropropanols are connected by dotted lines. For all functionals, dispersion correction was used.

However, vibrational frequencies are fully consistent between Cl without and Br with such a pseudopotential, as will be shown later on. If one assumes CCSD(T) to be most accurate, the chirality induction variation of the DFT predictions across Cl/Br and between 1-/2-ols is significantly too small. CAM-B3LYP and B2PLYP show the largest variations among DFT methods, but the magnitude of the chirality induction is overestimated. As illustrated in the ESI,† anharmonic zero point correction does not significantly influence the energy differences. Comparison to previous B3LYP and MP2 calculations for 1-X-propan-2-ols[93] with overestimated chirality induction effects indicate that dispersion correction for B3LYP and a saturated basis set for MP2 are essential. Previous MP2 calculations for Cl[10] also overestimate the 1-/2-ol difference in chirality induction. A direct comparison of all calculations can be found in the ESI.† In summary, 1-X-propan-2-ols show a stronger chirality induction on the torsional degrees of freedom than 2-X-propan-1-ols, and it remains unclear whether replacement of Cl by Br leads to a small or sizeable attenuation of the energetical chirality induction. Further high-level electron correlation studies would be helpful. The impact of temperature upon chirality induction appears to be rather small judging from Gibbs free energy calculations (default ORCA 4.2.1 settings incl. QRRHO[94]) at the B3LYP-D3(BJ,abc)/ma-def2-TZVP level, with entropic and enthalpic effects partially compensating each other (see ESI,† Fig. S2). The former favours the gG′ conformer, while the latter favours the g′G conformer.

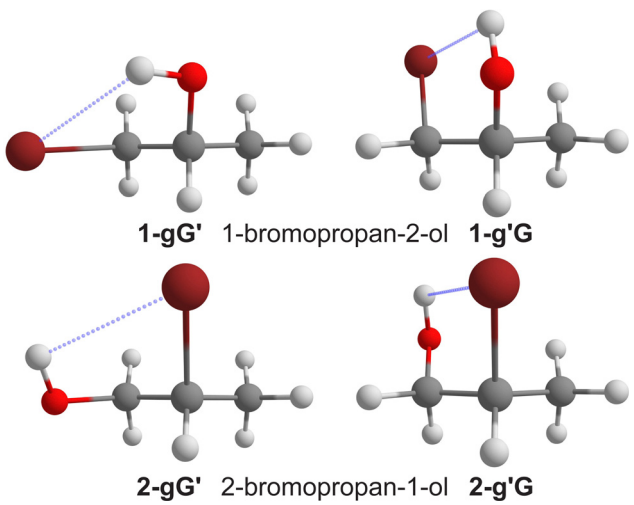

Fig. 2 Overview of the different conformers of *R*-configured 1-bromopropan-2-ol (top row) and 2-bromopropan-1-ol (bottom row). The corresponding chloro conformers are analogous in structure. The blue dotted lines indicate the hydrogen bonds/contacts. The conformers shown have been computed at the B3LYP-D3(BJ,abc)/ma-def2-TZVP level of computation.

3.2 Bromopropanol spectra

While theory more or less consistently predicts the energetic chirality induction effect to be larger for the secondary alcohols than for the primary alcohols, it has to be seen how this translates to spectroscopic observables such as OH stretching wavenumber shifts, rotational constants, and electrical field gradients at the halogen. We shall first discuss this for the so far unexplored Br derivatives, before recapitulating and extending the previous study of Cl derivatives.[10]

3.2.1 Raman spectroscopy. Fig. 3 shows the experimental as well as the harmonically predicted (and 0.96-scaled) Raman spectra of the bromopropanols. The computational level chosen is B3LYP-D3(BJ,abc)/ma-def2-TZVP, and relative intensities are Boltzmann scaled according to the corresponding relative energies. In case of 1-bromopropan-2-ol (black and dark grey), two distinct OH stretching bands can be easily identified, although the relative separation is underestimated by B3LYP. The signals at 3608 cm^{-1} and 3598 cm^{-1} can be assigned to gG′ and g′G, respectively. Unfortunately, only technical grade 1-bromopropan-2-ol was readily available with about 25% 2-bromopropan-1-ol as a contaminant (see ESI,† Table S3 for details of the compounds and gases used). In fact, a small shoulder of the band at 3608 cm^{-1} towards lower wavenumbers is most likely caused by 2-bromopropan-1-ol, as the red auxiliary trace shows. Hence, the predicted relative energies cannot be accurately assessed. For 2-bromopropan-1-ol (red and dark red), the picture is less clear as the OH stretching signals are predicted to be close together. Indeed, the single signal at 3607 cm^{-1} attributed to gG′ tails off towards higher wavenumbers. The shoulder at 3608 cm^{-1} is assigned to a minor contribution by g′G. Changes in the spectrum due to the different Br isotopes are very small and cannot be resolved.

In Fig. 4 the predicted conformational differences in hydrogen bond shift for the two conformations gG′ and g′G ($\Delta\tilde{\nu}$) are compared for all computational levels, circumventing the problem of absolute wavenumber prediction. Black and red

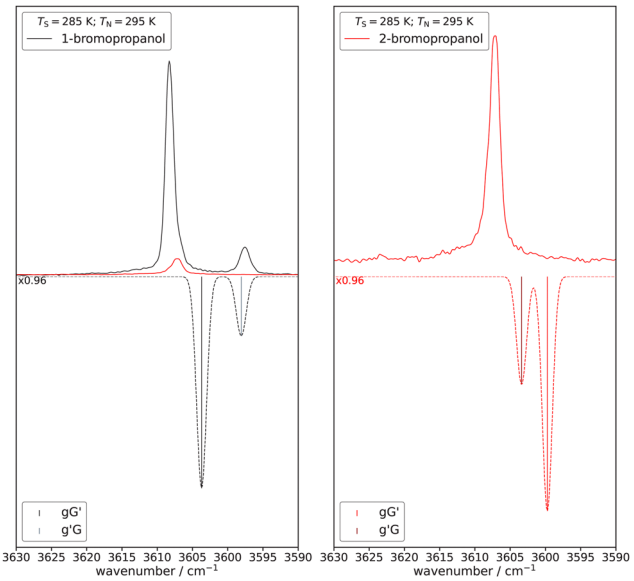

Fig. 3 Experimental Raman spectra (plotted upwards) and predictions at the B3LYP-D3(BJ,abc)/ma-def2-TZVP level (plotted downwards) of the bromopropanols. T_S refers to the saturator temperature and T_N to the nozzle temperature. The computed wavenumbers are uniformly scaled by 0.96 and the intensities are Boltzmann scaled according to T_N and to computed energies at the same level. An impurity of the 2-ol (right) in the 1-ol spectra (left, red) is indicated and elaborated on in more detail in the main text.

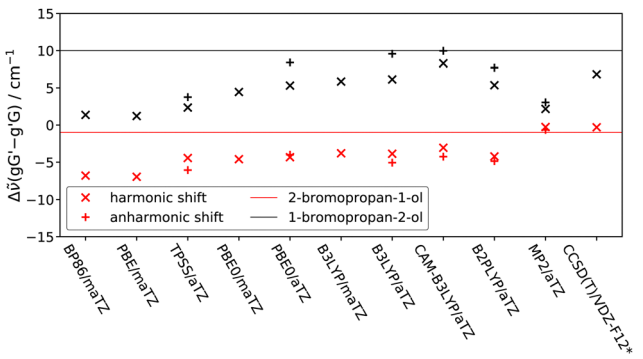

Fig. 4 Overview of the predicted harmonic (×) and anharmonic (+) conformational differences in the OH stretching wavenumbers. The experimental target values are indicated by the red and black line for 2-bromopropan-1-ol and 1-bromopropan-2-ol, respectively.

symbols refer to 2-bromopropan-1-ol and 1-bromopropan-2-ol, respectively. The experimental target values are indicated by the correspondingly coloured horizontal lines. Harmonically predicted differences are shown as × and anharmonically predicted differences as +. For harmonic predictions, it can immediately be seen that the BP86 and PBE GGA functionals yield the worst predictions out of all tested methods, predicting values that are consistently too small. The *meta*-GGA functional TPSS performs marginally better. The PBE0 and B3LYP hybrid functionals still predict somewhat too small differences. The range separated variant of B3LYP, *i.e.*, CAM-B3LYP, yields significantly better results for 1-bromopropan-2-ol. Results for the double hybrid functional B2PLYP more closely align with those of the regular hybrid functionals. Full MP2 also performs well for 2-bromopropan-1-ol but strongly underestimates the shift for 1-bromopropan-2-ol, yielding more similar results to the GGAs. Coupled cluster consistently performs well.

Anharmonic corrections are fairly small and tend to be counterproductive for 2-bromopropan-1-ol. Larger changes in the right direction are predicted for 1-bromopropan-2-ol, in particular for the hybrid functionals including the range separated one. Transferring the trends of the anharmonic correction to the harmonic coupled cluster results yields an improvement for either bromopropanol. This leads to essentially perfect spectral splitting predictions between the conformations in contrast to Fig. 3 based on B3LYP only.

With this added trust in the CCSD(T) performance, one can also interpret the relative intensities in terms of energy differences. For 2-bromopropan-1-ol, the spectral overlap does not allow to decide whether the B3LYP energy splitting is too large, as the CCSD(T) calculations imply. For 1-bromopropan-2-ol, where the energy predictions between the two methods are similar, the larger intensity ratio in experiment may hint at some relaxation from the g′G conformation to the gG′ conformation in the supersonic jet expansion.

The anharmonic calculations also invite a direct comparison of absolute wavenumbers with experiment. If harmonic predictions are to succeed in this comparison, they must predict harmonically too soft OH bonds. This is the case for the (*meta*)-GGA functionals listed in the upper part of Table 3, which provides wavenumber differences between theory and experiment. In such cases, VPT2 calculations are counterproductive, as illustrated for TPSS. Although the mean difference is fairly

Table 3 Overview of the difference between the predicted and experimental OH stretching wavenumbers for different computational methods of the bromopropanols. The upper part (BP86, PBE and TPSS) shows harmonic values and the effect of anharmonic correction for TPSS. The lower part shows further anharmonic predictions. For each method, the mean value as well as the standard deviation (σ) are shown. 1-gG′ and 1-g′G refer to 1-bromopropan-2-ol while 2-gG′ and 2-g′G refer to 2-bromopropan-1-ol. Positive values indicate overestimation and negative signs underestimation by a given method. All values are given in cm^{-1}

Harm	BP86	PBE	TPSS (harm/anh)
1-gG′	−6.0	4.7	22.5/−176.5
1-g′G	−0.2	10.7	25.9/−171.4
2-gG′	6.7	16.7	30.7/−165.0
2-g′G	−2.0	7.9	23.0/−171.3
Mean	−0.4	10.0	25.5/−171.0
σ	5.3	5.1	3.8/4.7

anh	PBE0	B3LYP	CAM-B3LYP	B2PLYP	MP2
1-gG′	11.0	−33.7	25.7	−14.9	−16.3
1-g′G	14.0	−29.6	29.0	−11.0	−16.7
2-gG′	18.8	−26.4	31.1	−12.0	−17.2
2-g′G	17.2	−26.9	31.1	−14.3	−24.1
Mean	15.3	−29.2	29.2	−13.1	−18.6
σ	3.5	3.3	2.5	1.8	3.7

low for the harmonic (*meta*)-GGA, the standard deviations (σ) are quite high showing that the error compensation is not so systematic. TPSS performs best, but expectedly breaks down when adding anharmonicity, both in terms of the mean and in terms of σ. Turning now to hybrid functionals which better capture the hardness of the OH bond (lower part of Table 3), anharmonic PBE0 overestimates the experimental results slightly which is in line with the fact that it generally predicts too stiff OH bonds. Rewardingly, σ is significantly smaller than was the case for the anharmonic TPSS. Anharmonic B3LYP underestimates the experiment but yields a similar σ as PBE0. CAM-B3LYP overestimates by similar amounts and further improves σ. B2PLYP improves on all three hybrid functionals, whereas MP2 is less consistent in its predictions. Given the very consistent deviations found for CAM-B3LYP and B2PLYP, an empirical wavenumber correction of −29 and +13 cm^{-1} can be introduced, respectively. The robustness of such a correction can later be tested with the chloropropanols.

3.2.2 Microwave spectroscopy. Microwave spectroscopy allows for the determination of a multitude of constants, especially since quadrupolar nuclei are present allowing for up to 16 different constants to be determined. However, the fitted nuclear spin-rotation interaction constants C_{aa}, C_{bb} and C_{cc} will not be discussed here and are beyond the scope of this work. For all conformers, the ^{79}Br and ^{81}Br isotopologues were fitted with all other isotopes being present in their naturally most abundant form. Furthermore, χ_{bc} could not be experimentally determined for 1-g′G and the CCSD(T)-DKH2 (CCSD(T)-DKH2/awCTZ//CCSD(T)-F12a/VDZ-F12*) values were used instead. The deviations of the tested methods relative to the experiment, as well as absolute deviations relative to the experimental values will be shown. It should be kept in mind that *A*, *B*, *C* and the nuclear quadrupole coupling constants (NQCC) were generally computed using the equilibrium geometry and not the vibrational ground state. Hence, good agreement with the experiment may not be for the right reason. However, in case of NQCCs, the VPT2 calculations indicate little change between the two. Similar observations were made previously by Stopkowicz *et al.*,[82] with the effect of DKH2 being significantly larger than vibrational ones. VPT2 also provides A_0, B_0 and C_0 values which also can be compared to experiment. All experimentally determined rotational constants can be found in the ESI.†

A comparison of the predictions for the rotational constants with the experiment is shown in Fig. 5. Here, predictions that are corrected for the vibrational ground state are indicated by a v_0 in front of the method. Otherwise the computations use the equilibrium structure. It is important to note that correct predictions that are based on the equilibrium structure may be right for the wrong reason. Conversely, wrong predictions may be wrong for the right reasons. For the predictions of *A*, it can be seen that the GGAs and *meta*-GGA behave very similar and underestimate *A*. However, the spread of the data is fairly small in comparison to the other tested methods. On the hybrid functional side, some stark differences between the functionals can be found. B3LYP yields predictions quite close to the experiment with the median (light blue circle) being very close to zero, for both the maTZ and aTZ basis sets. Additionally, the spread is very small. PBE0 and CAM-B3LYP overestimate the *A* rotational constant and show larger spreads. PBE0 shows especially large spreads. B2PLYP slightly overestimates and more closely resembles the results of B3LYP. In case of MP2, *A* is also overestimated. The datapoints around 90 MHz belong to the gG′ conformer of 1-bromopropan-2-ol. Coupled cluster shows even larger deviations of up to 140 MHz. This likely is a byproduct from the fact that equilibrium structures were used. As the A_0 results show, a switch to the ground state structure heavily influences *A*. Hence, CCSD(T) and MP2 are wrong for the right reasons. PBE0 and CAM-B3LYP perform especially well once vibrational averaging is taken into account. The good performance of B3LYP occurs for the wrong reason as it now significantly underestimates the experiment. To a lesser extent,

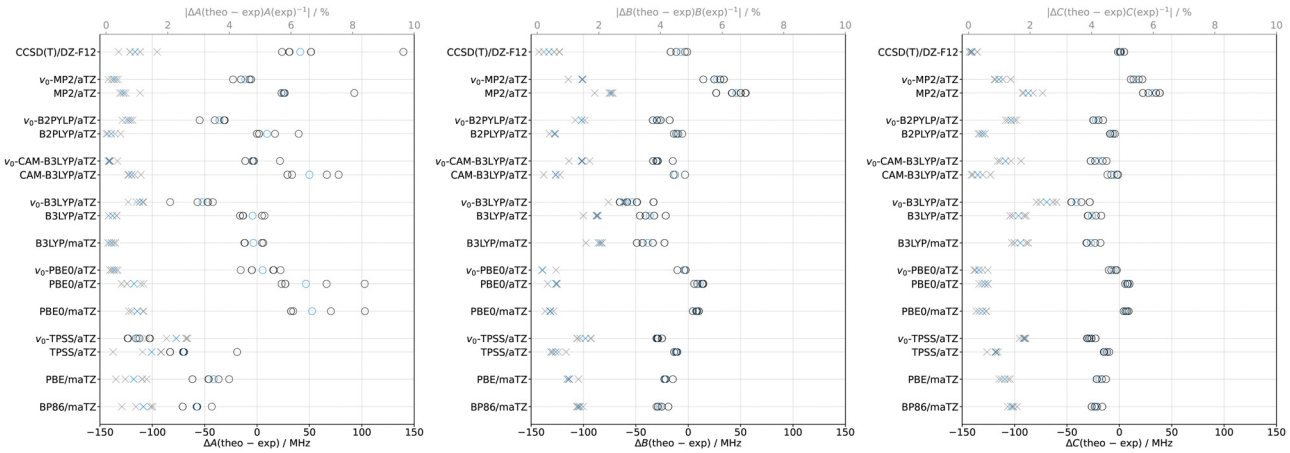

Fig. 5 Overview of the difference between the predicted and experimental values for the rotational constants *A*, *B*, and *C* for the bromopropanols. In cases where v_0 is added in front of a method, a vibrational ground state correction was applied while otherwise the equilibrium structure was used. In all cases, a total of eight data points are presented (black circles). Additionally, absolute relative deviations are shown with grey crosses using the grey *x*-axis at the top. The corresponding median values are given in blue.

this is also true for B2PLYP. In case of TPSS, this leads to an even stronger underestimation relative to the experiment. Furthermore, the spread is greatly reduced for PBE0, CAM-B3LYP and MP2. The experimentally determined A rotational constants range from 3944 MHz up to 8429 MHz. In this light, the deviations are fairly small in comparison to the experiment further corroborated by the absolute relative deviations shown in grey. However, the deviations are enough to lead to significant differences between the initial simulated and experimental spectrum. An example where A of the experimental fit of 2-gG′ is exchanged with the equilibrium value of the PBE0/aVTZ method is shown in the ESI,† to illustrate this point.

The predictions for B are generally closer to the experiment in absolute terms. Moreover, the spread of the data is significantly smaller. The (*meta*)-GGAs again underestimate the rotational constants but to a lesser extent than was the case for A. In case of TPSS, B is slightly underestimated. The predictions of B3LYP and PBE0 again significantly differ, with the former underestimating and the latter slightly overestimating B. The change in basis set has no significant influence on the predictions. Furthermore, B3LYP now shows a significantly larger spread of the data than PBE0, opposite to what was the case for A. CAM-B3LYP and B2PLYP show very similar results and slightly underestimate the experiment. For MP2, overestimation is found again. Coupled cluster now shows a very small spread and results that are very close to the experiment with a slight tendency towards underestimation. A comparison with the vibrational ground state results shows that the predictions change very little in absolute terms. Hence, good predictions at the equilibrium structure can still be considered to match for a physical reason. Interestingly, PBE0 again yields good results as was the case for A_0. MP2 and CAM-B3LYP also showed a good performance for A_0 but underestimate and overestimate B_0, respectively. The experimentally determined absolute values range from 1426 MHz up to 2349 MHz, and in relative terms the deviations from experiment are not substantial.

For the C rotational constant, the predictions are again closer to the experiment in absolute terms in comparison to A. The behaviour of the GGAs and the *meta*-GGA is again fairly similar with all of them underestimating C. PBE0 and B3LYP show very similar results as was the case for B. However, the spread of the data is slightly smaller. Yet again the change in basis set has no significant impact. For CAM-B3LYP and B2PLYP, the results are also similar to those found for B. In case of MP2, the overestimation is slightly attenuated in comparison to B. The CCSD(T) results are again remarkably close to the experiment. A comparison with the C_0 results shows that switching from the equilibrium to the ground state structure introduces only small changes, similarly to B_0. PBE0 yet again yields remarkably good predictions. The fact that PBE0 reproduces the experiment so well once vibrational averaging is taken into account indicates that it provides well balanced results that can be considered right for the right reasons or wrong for the right reason in case of the equilibrium results. However, this hinges upon the assumption that VPT2 is able to accurately predict vibrational ground state constants, which is not necessarily the case. The experimental values range from 1274 MHz up to 1676 MHz, and in relative terms the deviations from experiment are not significant.

As was previously mentioned, VPT2 calculations also provide quartic centrifugal distortion constants, *i.e.*, D_J, D_K, D_{JK}, d_1 and d_2. More details for their computation within the I^r representation and symmetric top (Watson S) reduction can be found in the ESI.† It is important to note that the centrifugal distortion constants obtained with VPT2 are equilibrium values and are based on a harmonic force field. Anharmonic effects are first included in VPT4, which is associated with an immense increase of computational cost in comparison to VPT2. Additionally, VPT4 implementations are generally not available in quantum chemistry programs. Therefore, only the computation of equilibrium values is feasible. Moreover, good agreement with the experiment may be due to error compensation of lacking anharmonic effects and deficits of the electronic structure calculations. A recent work by Franke and Stanton,[95] using a partial VPT4 implementation, suggests significant changes for D_K and D_{JK} in comparison to VPT2 for methanediol. These trends persist in both Watson′s A and S reduction. However, it remains unclear if this is caused by the partial nature of the implementation or anharmonic effects. Given the high level of electronic structure theory used by Franke and Stanton, issues arising from the correlation treatment are highly unlikely. Judging from Ray′s asymmetry parameter κ,[96] all conformers can be compared reasonably well to the very prolate methanediol ($\kappa \approx -0.93$[97]), with the exception of 2-gG′ ($\kappa \approx -0.34$). An overview of the deviation from experiment is shown in Fig. 6 for the different tested methods. When interpreting the data, it is crucial to keep the change of the order of magnitude in mind in comparison to the rotational constants. Experimental values as small as 0.181 kHz, 0.6930 kHz, 0.824 kHz, 0.00753 kHz and 0.00139 kHz are reached in terms of magnitude for D_J, D_K, D_{JK}, d_1 and d_2, respectively.

For D_J, TPSS and PBE0 show fairly large spreads with a tendency towards overestimation. B3LYP, CAM-B3LYP, and B2PLYP perform fairly similar clustering close to 0 kHz as indicated by the median. Overall, MP2 and CCSD(T) perform the best given their smaller spread. In comparison to the smallest experimental value of 0.18140 kHz, deviations of up to 0.04 kHz and 0.05 kHz of PBE0 and TPSS, respectively, are inadequate. The performance of the other methods is sufficient considering that most transitions are low J ones where the impact of D_J is still fairly small. In either case, using the D_J predictions for initial fits should help in the assignment process.

In case of D_K, all predictions tend towards overestimation with the exception of MP2 and CCSD(T). Furthermore, the spread of the data for TPSS is considerably larger than for all other tested methods. Curiously, coupled cluster also shows a large spread of the deviations only slightly smaller than those of TPSS. Considering that the smallest experimental value is 0.69300 kHz, no method is sufficiently accurate. However, with the exception of TPSS and arguably CCSD(T) all predictions yield the correct magnitudes. Moreover, all methods produce

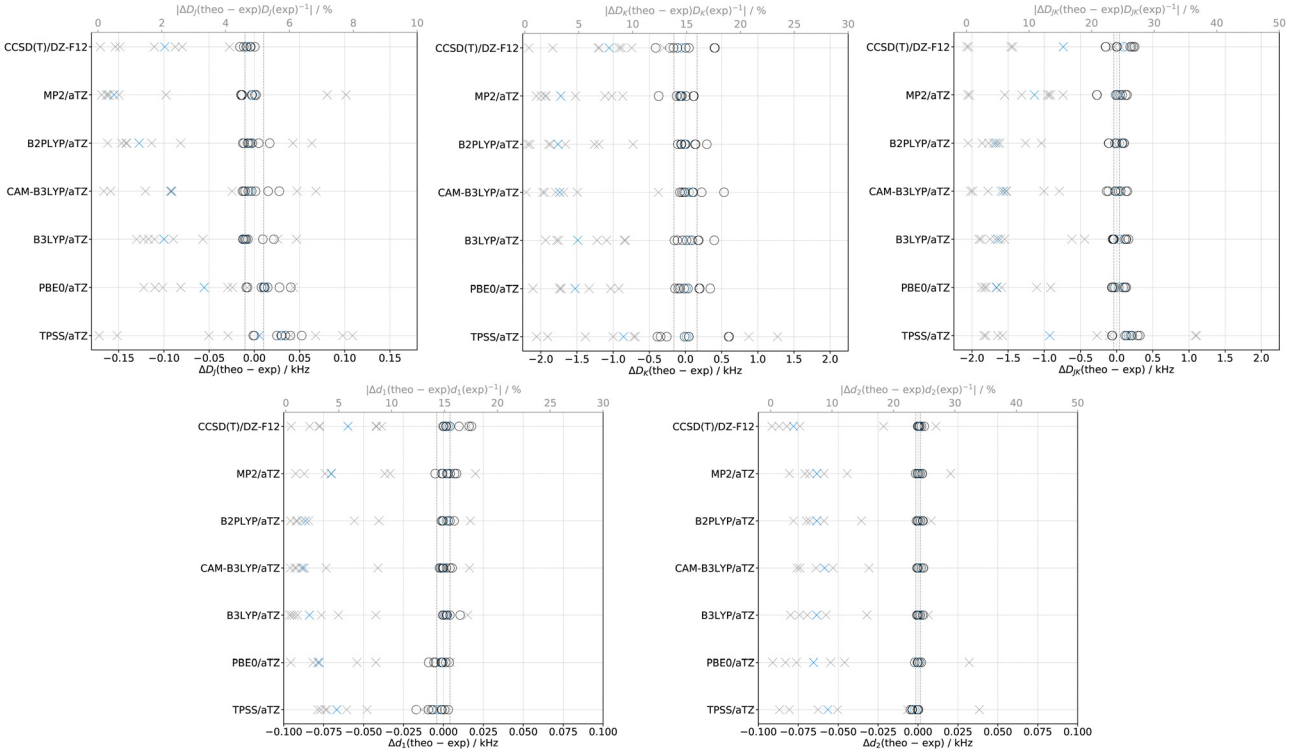

Fig. 6 Overview of the difference between the predicted and experimental values for the quartic centrifugal distortion constants D_J, D_K, D_{JK}, d_1 and d_2 for the bromopropanols. In all cases, a total of eight data points are presented (black circles) with the exception of d_2 where six are used. Additionally, absolute relative deviations are shown with grey crosses using the grey x-axis at the top. The corresponding median values are given in blue. The grey dashed vertical lines represent the largest experimental uncertainties.

the correct sign, which can be of great help in case of ambiguous assignments.

The predictions for D_{JK} appear to be more reliable again in comparison to D_K. Experimentally, both of them span a very similar range of magnitude. Hence, all methods can be considered reasonably accurate with TPSS showing deviations at most of about 40% of the smallest experimental D_{JK} value. Although this is still a significant amount, it is sufficient to aid the assignment of rotational spectra. In all cases, the correct order of magnitude and sign were predicted by the tested methods. Overall, no clear recommendation can be made with PBE0, B3LYP, CAM-B3LYP, and B2PLYP performing equally well.

For the off-diagonal quartic centrifugal distortion constants d_1 and d_2, the smallest experimental reference values are two orders of magnitude smaller than the diagonal quartic centrifugal distortion constants (D_J, D_K, D_{JK}). In case of d_1, the deviations are substantial in comparison to the experimental values. This is especially true for TPSS and coupled cluster, although these methods deviate in different directions. Overall, CAM-B3LYP performs the best – closely followed by B2PLYP and MP2. However, yet again the predictions generally match the order of magnitude and in all cases predict the correct sign. For d_2, the seemingly smaller deviations in comparison to d_1 arise from the fact that d_2 is generally smaller. Similarly to d_1, the deviations for d_2 are comparatively large with regards to the experimental values, as indicated by the absolute relative deviations. Regardless, the predictions still provide utility since the signs and order of magnitude are predicted correctly. It is also worth pointing out that of the distortion constants, d_2 usually has the largest experimental uncertainty. Hence, the predictions may in actuality be better than they seem. Overall, PBE0 yields the best predictions and TPSS the worst. The other tested methods perform about the same.

Lastly, the predictions for χ_{aa}, χ_{bb-cc}, χ_{ab}, χ_{ac} and χ_{bc} will be compared to the experiment. Since the sign of the off-diagonal elements is not clearly defined, the modulus will be used instead. Hence, a description in terms of under- or overestimation is not possible. It should also be kept in mind that although the electric field gradient might be predicted correctly by a given method, the projection to the inertial principal axis system may introduce deviations from experiment.[98] This may lead to error compensation or error compounding. The results are shown in Fig. 7. For χ_{aa}, all methods, with the exception of CCSD(T)-D(KH2), underestimate the experimental value. Especially MP2 shows this tendency. While for A, B and C the change in basis set for B3LYP and PBE0 did not lead to significant changes (see Fig. 5), here, the maTZ basis set performs better. Overall, B3LYP/maTZ performs best. Curiously, the GGAs yield results on par with the non-relativistic coupled cluster calculations. The deviations appear to be fairly consistent so that an empirical correction could be derived. Furthermore, significant differences can be found between the DKH2 and non-relativistic coupled cluster results indicating that relativistic

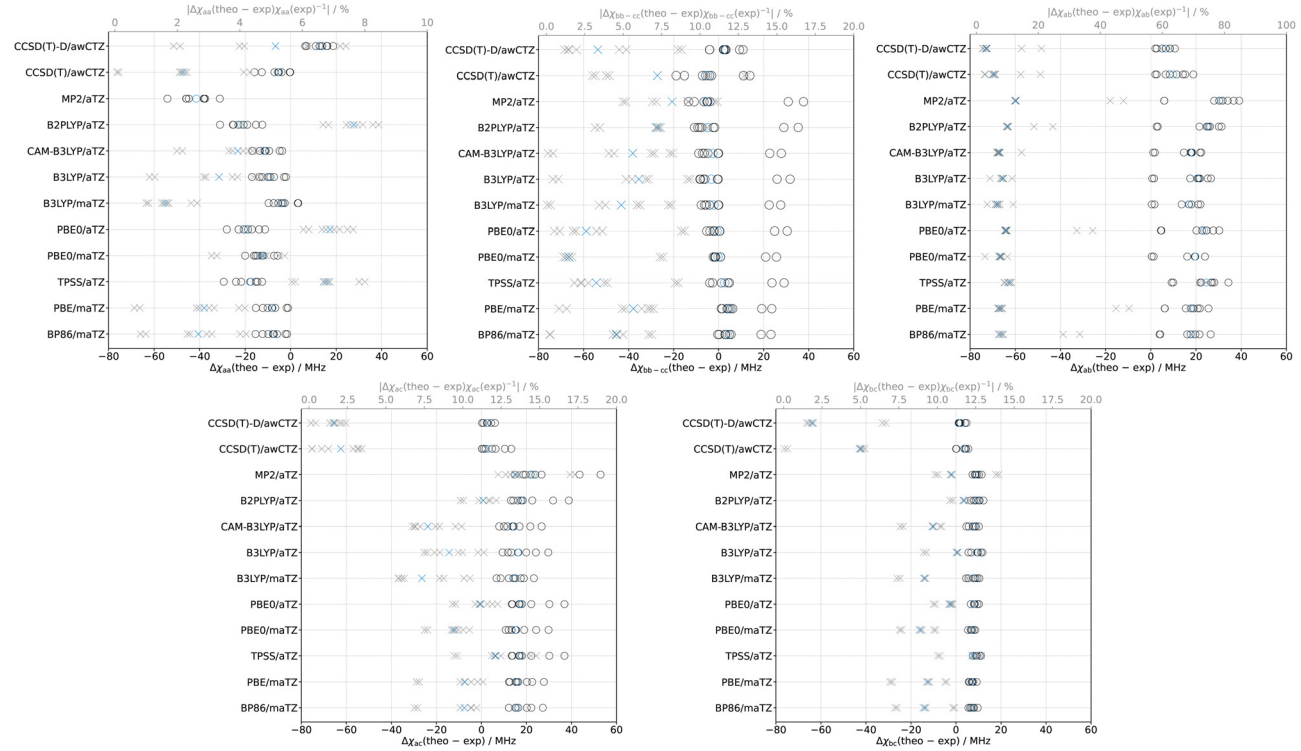

Fig. 7 Overview of the difference between the predicted and experimental values for the nuclear quadrupole coupling constants χ_{aa}, χ_{bb-cc}, χ_{ab}, χ_{ac} and χ_{bc} for the bromopropanols. -D indicates the use of DKH2. In all cases a total of eight data points are presented (black circles) with the exception of χ_{bc} where six are used. Additionally, absolute relative deviations are shown with grey crosses using the grey x-axis at the top. The corresponding median values are given in blue. The grey dashed vertical lines represent the largest experimental uncertainties.

effects are relevant. However, it appears as if DKH2 may overcorrect leading to an overestimation of χ_{aa} although the spread of the data is reduced. The use of specialised DKH2 basis sets may remedy this discrepancy. In general, the performance of most methods is adequate considering that the experimental values range from 187 MHz to 367 MHz.

In case of χ_{bb-cc}, the average deviations tend to be much closer to 0 MHz than was the case for χ_{aa}. However, the spread of the data is significantly increased with the exception of CCSD(T)-D. Furthermore, most methods show a pair of datapoints close to or above 20 MHz, which is caused by the gG′ conformer of 1-bromopropan-2-ol. This could be related to the fact that for the more stable gG′ conformer the Br atom lies within the plane spanned by the C–C–C backbone, while for the less stable g′G it is approximately orthogonal to the backbone plane (*cf.* Fig. 2). For 2-bromopropan-1-ol, the Br atom is always pointing outside of the C–C–C plane. Overall, CCSD(T)-D performs the best. Furthermore, including DKH2 again leads to a decrease in the spread of the data. Changes in the basis set appear to be less relevant than was the case for χ_{aa}. The experimental data covers a range from 56 MHz to 339 MHz in absolute terms. Keeping this in mind, all methods with the exception of CCSD(T)-D are not sufficiently accurate.

For χ_{ab}, no judgement can be made with regards to over- or underestimation. Most methods show a fairly large spread of the data. Yet again, CCSD(T)-D has the smallest spread by far followed by its non-relativistic variant. MP2 shows the largest spread and deviations as was the case for χ_{aa} and χ_{bb-cc}. This is especially significant since experimental values as low as 14 MHz (1-g′G conformer) have been determined. This is further illustrated by the relative absolute deviations. Hence, all methods in principle are not sufficiently accurate. However, all other conformers have values above 200 MHz, for which the tested methods would suffice.

In the case of χ_{ac}, the CCSD(T)-D calculations are remarkably accurate significantly outperforming all other methods. Non-relativistic coupled cluster performs worse but better than the remaining methods. These methods mostly centre around 20 MHz as indicated by the median. Yet again MP2 shows the largest deviations and spread. PBE and BP86 have a fairly small spread similar to the χ_{aa} case, and an empiric correction could provide a computationally cheap alternative to coupled cluster calculations. The outliers are again due to the 1-g′G conformer. However, MP2, B2PLYP, PBE0 and TPSS still struggle in its description whereas for χ_{bb-cc} only the coupled cluster methods did not show outliers. Moreover, in terms of magnitude the smallest experimental value is 115.32 MHz so that most methods can be considered reasonably accurate.

The predictions for χ_{bc} stick out in comparison to the rest due to the very small spread of the data for all methods. This is especially true for BP86 and PBE again making an empirical correction very promising. Surprisingly, even MP2 shows a very small spread, which previously behaved quite inconsistently. In terms of their predictive capabilities, CCSD(T)-D performs the

best closely followed by its non-relativistic variant. The other methods tend to deviate by about 10 MHz. The experimental values for χ_{bc} range from 61 MHz up to 104 MHz in magnitude. Therefore, all methods can be considered reasonably accurate. χ_{bc} of the 1-g′G conformer could not be experimentally determined. Given that CCSD(T)-D predicts very small values of −1.438 and −1.216 MHz for ^{79}Br and ^{81}Br, respectively, this can be rationalised. It also shows that despite bromine's large quadrupole moment and electric field gradient, the transformation to the inertial principal axis system can result in very small χ.

3.3 Chloropropanol spectra

In the good practice of benchmarking,[99] this study was extended to include the chlorinated analogues of the propanols. The novel Raman results are presented here, along with rotational spectroscopy data to extend the work of Goldstein *et al.*[10] As will be detailed later, the results of the bromopropanol study lead to a promising possible correlation between the OH stretching frequencies and the change in asymmetry of the halogen electric field gradient, η. This correlation can now be compared with both the respective chlorine and bromine containing propanols.

3.3.1 Raman spectroscopy. In case of the chloropropanols, pure samples could be easily obtained allowing for more quantitative judgement of the predicted relative energies. Fig. 8 shows the experimental as well as the predicted Raman spectra of the chloropropanols. The spectral pattern is very similar to the bromopropanols (*cf.* Fig. 3) with a consistent shift of about 10 cm^{-1} towards higher wavenumbers indicating that the OH···Br contacts are stronger than their Cl counterparts. The same scaling factor that was used for the bromopropanols (0.96) was applied here. For 1-chloropropan-2-ol, gG′ can be assigned to the strong signal at 3619 cm^{-1} and g′G to the smaller one at 3609 cm^{-1}. In case of 2-bromopropan-1-ol, a single strongly asymmetric band was observed (*cf.* Fig. 3) whereas in the Cl case the single signal is very slightly asymmetric. This may be due to a stronger spectral overlap of gG′ and g′G and/or due to g′G being more strongly populated in the Br case as the coupled cluster calculations would suggest (see Fig. 1). Considering these aspects, it is assumed that gG′ and g′G overlap yielding a combined signal at 3620 cm^{-1}. As was the case for the bromopropanols, spectral differences due to ^{35}Cl and ^{37}Cl cannot be resolved.

A comparison between the predicted and the experimental hydrogen bond shifts can again be made. The results are remarkably similar to the bromopropanols (see Fig. 4). A detailed discussion can be found in the ESI† (Section 6).

Since both chloro- and bromopropanols are vibrationally characterised, the induced shift due to the different halogens can also be analysed. Such a comparison is shown in Fig. 9 for the 2-ol (top) and 1-ol (bottom). In all cases, the Cl analogues have higher OH stretching frequencies resulting in positive shifts ($\tilde{\nu}_{OH}$ (1/2-Cl) − $\tilde{\nu}_{OH}$ (1/2-Br)). The experimental substitution shifts are very consistent ranging from 11–13 cm^{-1}. Similarly, the predictions are also fairly analogous. The (*meta*)-GGAs significantly overestimate the impact of bromination – predicting values about twice as large as the experiment.

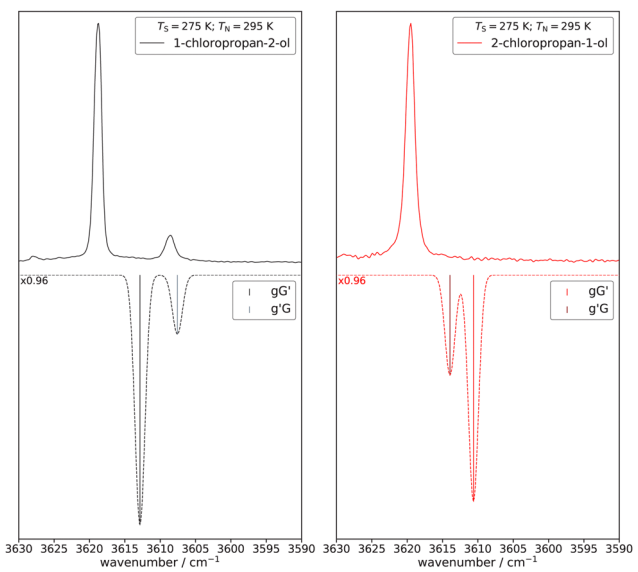

Fig. 8 Experimental Raman spectra (plotted upwards) and the scaled predictions at the B3LYP-D3(BJ,abc)/ma-def2-TZVP level of theory (plotted downwards) of the chloropropanols. The spectra are scaled by 0.96 in either case. T_S refers to the saturator temperature and T_N to the nozzle temperature. The experimental intensities are Boltzmann scaled according to T_N and the relative energies computed at the B3LYP-D3(BJ,abc)/ma-def2-TZVP level.

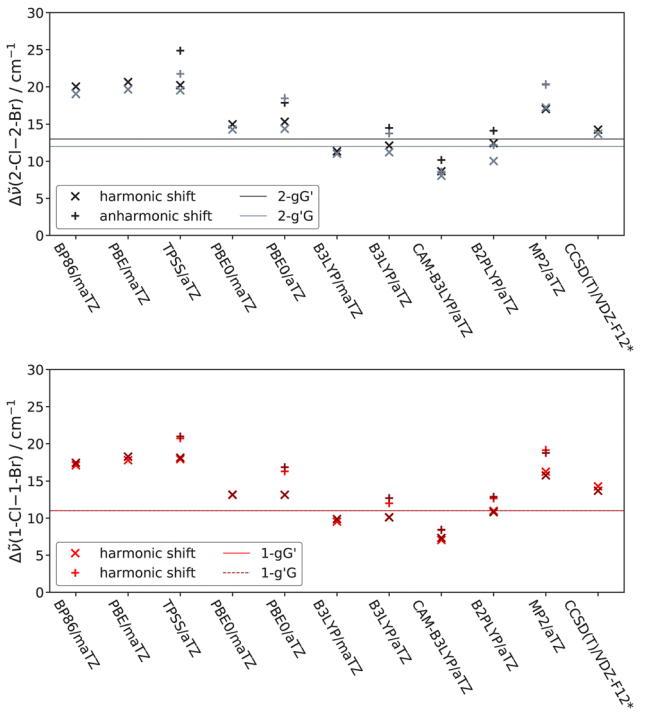

Fig. 9 Overview of the predicted harmonic (×) and anharmonic (+) shifts between the OH stretching frequencies of the Br and Cl analogues. The experimental values are indicated by the black/grey and red/dark red line for 2-X-propan-1-ol and 1-X-propan-2-ol, respectively.

The hybrid functionals provide a significant improvement with B3LYP performing especially well. Out of these functionals, CAM-B3LYP performs the worst slightly underestimating the shift introduced by the change of halogen. B2PLYP also performs quite well but somewhat overestimates the separation of the gG′ and g′G conformers. As was the case for the shift between conformers (see Fig. 4 and Fig. S3 of the ESI†), MP2 shows very similar behaviour as the (*meta*)-GGAs. Coupled cluster performs very well for the 2-ols with some slightly larger deviations from experiment for the 1-ol. Of the tested methods, PBE0 most closely reproduces the CCSD(T) results. The anharmonic corrections consistently result in larger halogen introduced shifts, which leads to a worse agreement with experiment for all methods except CAM-B3LYP.

The absolute band predictions can also be analysed with regards to their predictive capabilities. In general, the results are quite similar to those of the bromopropanols (see Table 3) and a detailed analysis can be found in the ESI† (Section 6). Crucially, B2PLYP shows very consistent deviations from experiment with an empiric correction derived from the bromopropanols (+13 cm^{-1}) yielding excellent results. To a lesser extent this is also true for CAM-B3LYP and B3LYP. This correction could be extended to more complex 3-chloro- and 3-bromopropane-1,2-diols.

3.3.2 Microwave spectroscopy. The microwave analysis is based on the lines reported by Goldstein *et al.*[10] with some additional lines being measured and remeasured by us using the cavity setup in Göttingen (so called Q-CUMBER) to improve the accuracy of the χ-tensor. Furthermore, χ_{ab} and χ_{bc} could not be experimentally determined for 1-g′G, as well as χ_{ac} for 2-gG′. For these instances, the CCSD(T)-DKH2(CCSD(T)-DKH2/awCTZ//CCSD(T)-F12a/VDZ-F12) value was used instead. Fig. 10 shows the deviations from experiment where methods with an added v_0 use vibrationally averaged structures. For all other methods, the equilibrium structure was used.

For *A* based on equilibrium geometries, it can be seen that in comparison to the bromopropanols the spread of the data is significantly larger with the exception of CCSD(T) (*cf.* Fig. 5). The behaviour of coupled cluster can be attributed to the fact that *A* of the 1-gG′ conformer is not as strongly overestimated as was the case for 1-bromopropan-2-ol. While for the bromopropanols CCSD(T) overestimated the results considerably and exhibited very large spreads, the spread is strongly reduced for the chloropropanols, and the predicted values match well to the experiment. In fact, coupled cluster yields the best results of all tested methods. Previously B3LYP performed best, however, it now underestimates *A* significantly for some conformers. Coupled cluster is followed in terms of predictive capabilities by B2PLYP. Unfortunately, either method is computationally fairly expensive. Curiously, the very cheap BP86 and PBE functionals show very similar deviations and spreads as was the case for the bromopropanols. Hence, an empirical back correction would yield good results at very small cost. Furthermore, given the smaller mass of Cl, the experimental values for *A*, *B* and *C* are larger than for their bromine counterparts. Hence, relatively speaking, the deviations from experiment are less significant.

In case of *B*, again quite similar deviations can be found as was the case for the bromopropanols. Moreover, the spread of the data also increases again. CCSD(T) yields good predictions with a very small spread. CAM-B3LYP also performs very well with a somewhat larger spread. Furthermore, BP86 and PBE show great potential again for an empirical back correction based on the bromopropanol results. This could also be done for PBE0 and B3LYP but the low computational costs makes the GGAs especially attractive.

For *C*, similar behaviour to the bromopropanols can again be found. As for *B*, the performance of coupled cluster is quite good followed by CAM-B3LYP. In comparison to the bromopropanols, the spreads are again slightly larger. PBE and BP86 lend themselves for a back-correction as they behave very consistently and show fairly small spreads of the data. B3LYP and MP2 would also benefit from such a correction, however, given

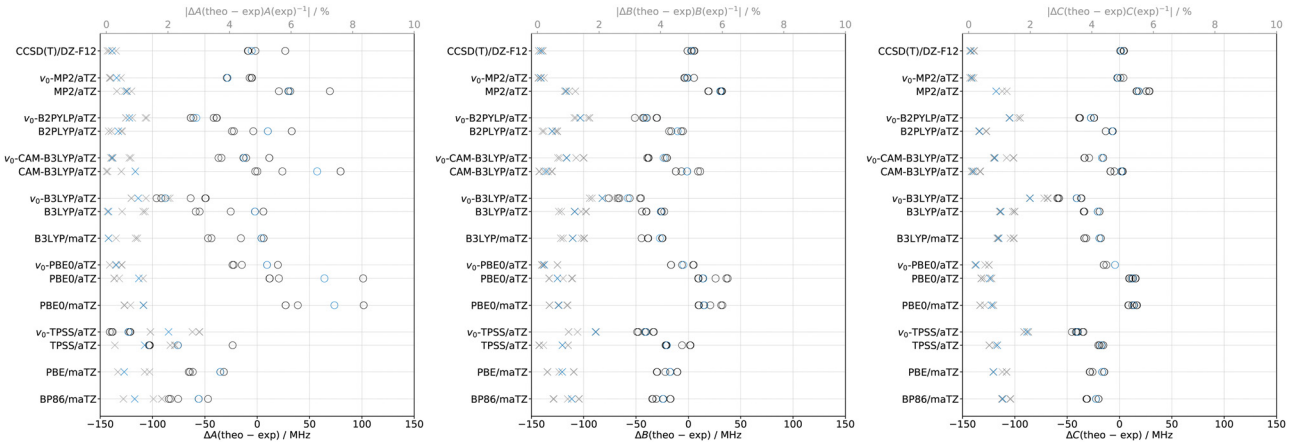

Fig. 10 Overview of the difference between the predicted and experimental values for the rotational constants *A*, *B*, and *C* for the chloropropanols. In cases where v_0 is added in front of a method, a vibrational ground state correction was applied while otherwise the equilibrium structure was used. In all cases a total of eight data points are presented (black circles). Additionally, absolute relative deviations are shown with grey crosses using the grey *x*-axis at the top. The corresponding median values are given in blue.

the computational cost the GGAs are preferable. An interesting test case for such a back-correction are the corresponding iodopropanols, which can be studied in the future.

The addition of vibrational averaging reduces the spread of the data as was the case before. However, in a direct comparison the spreads are slightly smaller for the bromopropanols. For A, once again all methods, with the exception of PBE0, tend to underestimate the experimental results. In comparison to the bromopropanols, this downshift is slightly more pronounced. PBE0 predicts values close to experiment, as was previously observed. Furthermore, all methods predict a rough average downshift of 50 MHz relative to their equilibrium geometries. Similar observations can also be made for the bromopropanols. Extrapolating this to the equilibrium coupled cluster results of the chloropropanols would indicate that its predictions should be larger. In fact, it appears as if the results are right but likely for the wrong reasons. However, it may also be the case that VPT2 overestimates the influence of vibrational ground state effects for the chlorine derivatives.

In case of B_0, the vibrational averaging again has less of an impact compared to A_0. The spread of the data is also slightly reduced. Most methods underestimate B_0 in comparison to the experiment. PBE0 does so only slightly and is performing quite well again. Interestingly, MP2 yields a good match with the experiment, whereas it overestimated B_0 for the bromopropanols. This can be attributed to the fact that the equilibrium results for the chloropropanols are lower leading to a match once the vibrational ground state is accounted for. Similar behaviour can also be found for C_0, where MP2 again yields predictions remarkably close to the experiment. All other methods show results that are too small. However, once again PBE0 does so only very slightly deviating by −15 MHz at most. At the equilibrium geometry PBE0 deviates at most by +15 MHz. Moreover, PBE0 consistently provides good predictions for A_0, B_0 and C_0 for the bromo- and chloropropanols. Given that PBE0 is still reasonably cheap, it could also be tested for its capabilities for larger systems. For instance, a VPT2 calculation using PBE0 takes around 15 hours for the chloropropanols and around 17 hours for the bromopropanols using 18 cores (Intel Xeon Gold6240(18)@3.9 GHz). Methods such as B2PLYP are far more limited with a VPT2 calculation taking about 5 days using twice the amount of cores.

Similar to the bromopropanols, the quartic centrifugal distortion constants are several orders of magnitude smaller than the rotational constants. Experimentally, values as small as 1.13 kHz, 2.06 kHz, 5.49 kHz, 0.500 kHz and 0.0948 kHz have been determined in absolute terms for D_J, D_K, D_{JK}, d_1 and d_2, respectively. In comparison to the bromopropanols, these values are generally larger. The deviations from experiment for the distortion constants is shown in Fig. 11. For D_J, satisfactory agreement between experiment and theory can be found with most methods having a median close to 0 kHz and a

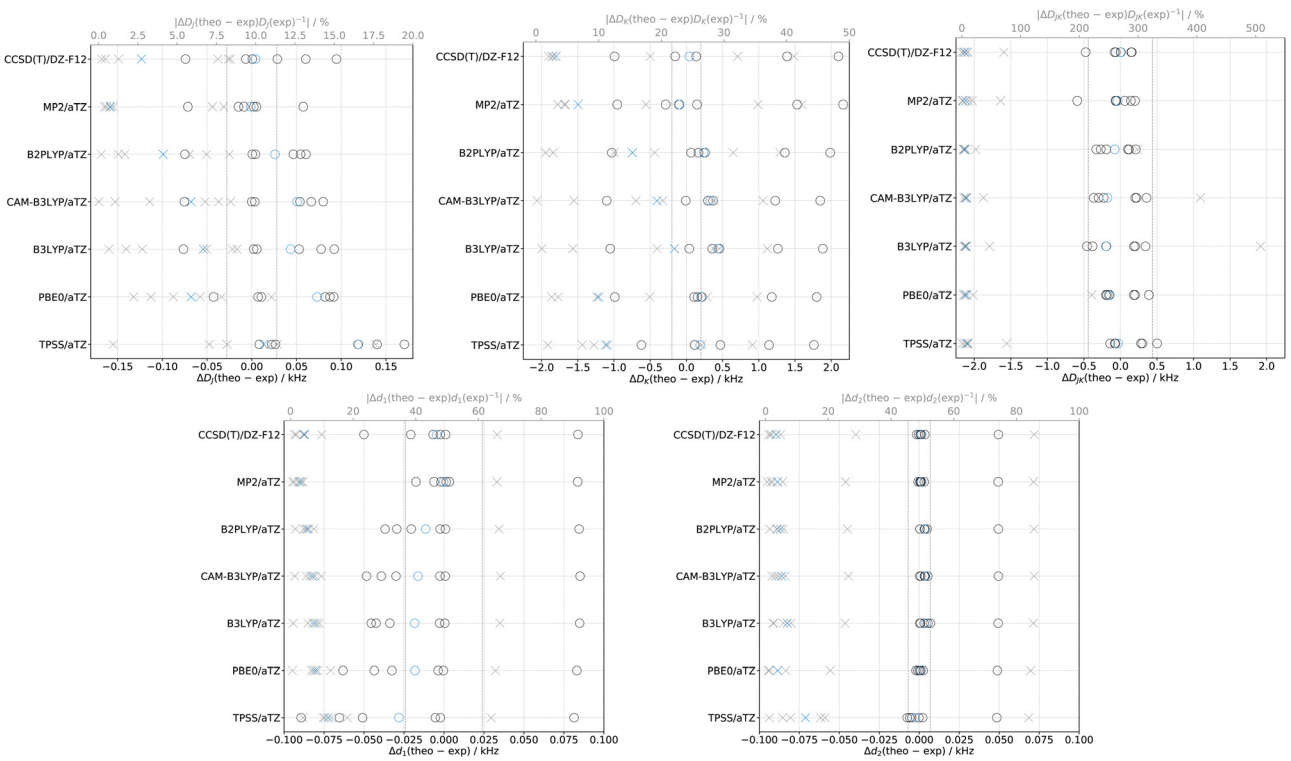

Fig. 11 Overview of the difference between the predicted and experimental values for the quartic centrifugal distortion constants D_J, D_K, D_{JK}, d_1 and d_2 for the chloropropanols. For D_J, D_K and D_{JK}, seven data points (black circles) are used while for d_1 and d_2 six are included. Additionally, absolute relative deviations are shown with grey crosses using the grey x-axis at the top. The corresponding median values are given in blue. The grey dashed vertical lines represent the largest experimental uncertainties.

significantly smaller spread than the smallest experimental value. Moreover, the largest experimental uncertainties are quite close to the deviation from experiment, especially for MP2. In case of D_K, quite substantial deviations can be found which was already the case for the bromopropanols (*cf.* Fig. 6). As was previously the case, all methods tend to overestimate D_K slightly. Considering that values as small as 2.064 kHz have been experimentally determined, the results are not satisfactory in terms of their predictive capabilities. Deviations from the experiment can reach values about twice as large as the largest experimental error. However, in all cases the correct order of magnitude and sign was predicted which can be of great help for difficult assignments. For D_{JK}, larger deviations from experiment can be found in comparison to the bromopropanols while the tendency towards slight overestimation is kept. Here, the agreement with the experiment is not satisfactory considering the order of magnitude of the experimental values. However, deviations from experiment stay within the largest experimental error for most tested methods. Moreover, the predictions for 1-g′G (^{35}Cl) are especially bad for MP2 and CCSD(T) with values around −0.5 kHz. Furthermore, the relative absolute deviations are exceptionally large for 2-gG′ (^{35}Cl) with values as high as 500%. Some of the large differences may be due to the relatively large experimental uncertainty. The larger discrepancies for D_K and D_{JK} may again be attributed to the lack of vibrational effects in VPT2 as observed by Franke and Stanton for methanediol.[95] However, 2-gG′ ($\kappa \approx -0.05$) and 2-g′G ($\kappa \approx -0.40$) more closely resemble an asymmetric rotor and comparability to the prolate methanediol ($\kappa \approx -0.93$[97]) may be limited in those cases. The strong asymmetry might also explain the large absolute relative deviations for D_{JK}.

For the off-diagonal quartic distortion constants, good agreement between experiment and theory can be found for d_2 while significant deviations can be observed for d_1. For the former, good results are provided by MP2, which yields deviations significantly smaller than the smallest experimental value as well as the largest experimental uncertainty. In either case, a substantial outlier can be observed belonging to 1-g′G. Here, the sign is predicted correctly but the order of magnitude does not match. However, excluding this data point, MP2 again provides accurate predictions. It may be the case, that despite a fairly small statistical error, d_1 and d_2 are not properly converged yet. TPSS and PBE0 yield deviations that are too large to be considered accurate given the smallest experimental value. Given the largest experimental error, they are still good enough to provide starting points for initial fits. The overall larger experimental errors and deviations from experiment of the chloropropanols in comparison to the bromopropanols can be at least partially attributed to the fact that higher quantum numbers J, K_a, K_c and F can be reached (for J, K_c and F *ca.* +3 on average, K_a only slightly changes) as well as more lines being included in the fit.

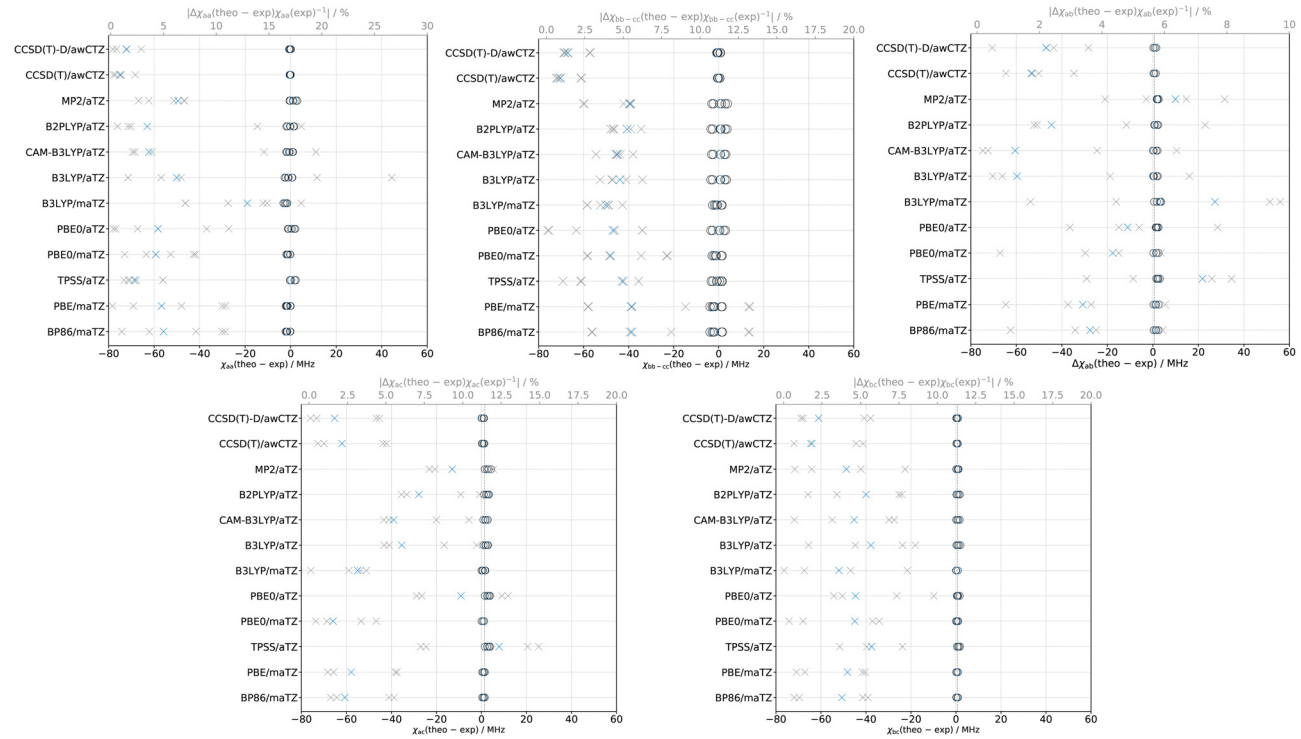

Fig. 12 Overview of the difference between the predicted and experimental values for the nuclear quadrupole coupling constants χ_{aa}, χ_{bb-cc}, χ_{ab}, χ_{ac} and χ_{bc} for the chloropropanols. -D indicates the use of DKH2. For χ_{aa} and χ_{bb-cc}, eight data points are used (black circles) while for χ_{ab}, χ_{ac} and χ_{bc} five are included. Additionally, absolute relative deviations are presented with grey crosses using the grey x-axis at the top. The corresponding median values are given in blue. The grey dashed vertical lines represent the largest experimental uncertainties. The latter is only shown for χ_{ab}, χ_{ac} and χ_{bc} since here significant uncertainties are present.

Due to Q being significantly smaller for ^{35}Cl (Q = −0.0817 barn) and ^{37}Cl (Q = −0.0644 barn) than for ^{79}Br (Q = 0.313 barn) and ^{81}Br (Q = 0.262 barn),[90] χ_{ij} is also smaller. The electric field gradient is also reduced for chlorine but this change is not as impactful as the change in Q. The differences between theory and experiment are shown in Fig. 12. For χ_{aa}, seemingly excellent agreement can be observed for all methods with most of them tending towards a slight underestimation of the experiment. However, considering that values as small as 8.2 MHz are reached, most methods are insufficiently accurate. Of the density functionals, B2PLYP and CAM-B3LYP yield good results. Coupled cluster yields predictions that are remarkably close to the experiment deviating at most by about 0.5 MHz. Moreover, as one might expect, relativistic effects do not play a significant role with the DKH2 predictions being almost identical to the non-relativistic ones. This may be seen as a trivial observation, nonetheless, it is worthwhile checking if DKH2 reproduces what one might purely infer from chemical intuition. Furthermore, whereas for A, B and C consistent deviations between the halogenated propanols were found, this is no longer the case for χ_{ij} (*cf.* Fig. 7). However, similarities to other chlorinated alcohols may be found as goes for other brominated alcohols in case of the bromopropanols.

In case of χ_{bb-cc}, deviations are again seemingly small with a tendency towards underestimation. Here, the smallest determined experimental value is 13.95 MHz in terms of magnitude. Of the tested methods, B3LYP/aTZ and PBE0/aTZ show the largest deviations with *ca.* −3.5 MHz, which is still reasonably small in comparison to the smallest experimental value. Coupled cluster again performs exceptionally well with no significant difference between the DKH2 and non-relativistic results. For both variants, deviations stay well within 1 MHz. Furthermore, most tested methods struggled to predict χ_{bb-cc} for the g′G conformer of 1-bromopropan-2-ol, which is no longer the case here. However, problematic behaviour may be masked by the change in the order of magnitude (^{79}Br: −338.5 MHz *vs.* ^{35}Cl: 55.6 MHz).

For χ_{ab}, no judgement with regards to over- and underestimation can be made. The smallest determined experimental value is 31.6 MHz. The deviations of the tested methods are considerably smaller, therefore, all methods are sufficiently accurate. Coupled cluster again yields very good results, however, a similar degree of accuracy can also be reached with the much cheaper BP86 and PBE functionals. It is also worth noting that χ_{ab} of the 1-g′G conformer could not be determined. Here, coupled cluster predicts very small values around 1.7 MHz, which would potentially provide a challenge for theory if it were determined. For the bromine analogues, very small values were determined which indicates that values around 1.7 MHz are reasonable. Additionally, fits including χ_{ab} in the Hamiltonian converge for 1-g′G, however, χ_{ab} can be manually set to different values without impacting the quality of the fit. Hence, χ_{ab} is clearly not well determined and was not used in the fit. Goldstein *et al.*[10] included χ_{ab} in their fits for ^{35}Cl.

In case of χac, generally good agreement between experiment and theory can be found. Considering that the smallest experimental value was determined to be 15.4 MHz, methods such as MP2/aTZ, PBE0/aTZ and TPSS/aTZ with deviations of up to 4 MHz are not as well suited as the others. Furthermore, calculations utilising the maTZ basis set perform better than their aTZ counterpart. Of all tested methods, CCSD(T) performs best – closely followed by the GGAs.

For χ_{bc}, good agreement between experiment and theory can again be found. Coupled cluster performs exceptionally well but similar accuracy can again be achieved with the much cheaper BP86 and PBE functionals. Considering that the smallest fitted value was 8.6 MHz, some methods such as B3LYP/aTZ may be considered insufficiently accurate with a maximum deviation of about 2 MHz. Additionally, Goldstein *et al.*[10] included χ_{bc} in their fit for the 1-g′G conformer for ^{35}Cl. In our fits, χ_{bc} was not included due to the same reason stated for χ_{ab}. Moreover, the best predictions available indicate values below 1 MHz already indicating that a well determined fit would be very challenging. Furthermore, even for the bromine analogue it could not be determined. Given this fact, it is even more clear that χ_{bc} cannot be determined for 1-g′G in the chlorine case.

3.4 Combining rotational and vibrational spectroscopy

Rotational spectroscopy allows for the derivation of direct information about the electronic environment at a quadrupolar nucleus. This can be done by converting the χ_{ij}-tensor from the inertial principal axis system (see eqn (3)) to that of the nucleus. This can be achieved by diagonalisation of the tensor yielding χ_{xx}, χ_{xx} and χ_{zz}, which are also traceless. The diagonalisation was done with Z. Kisiel′s QDIAG programme (Version 12.II.2023).[100]

$$\chi_{ij} = \begin{pmatrix} \chi_{aa} & \chi_{ba} & \chi_{ca} \\ \chi_{ab} & \chi_{bb} & \chi_{cb} \\ \chi_{ac} & \chi_{bc} & \chi_{cc} \end{pmatrix} \quad (3)$$

In principle, six permutations for the mapping of a, b and c to x, y and z are possible. It is convention to choose the axis system such that $|\chi_{xx}| \leq |\chi_{yy}| \leq |\chi_{zz}|$. For the systems studied here, χ_{zz} approximately points in the direction of the C–Cl or C–Br bond since the electric field gradient is largest in that direction. From these χ values the asymmetry parameter η of the nuclear quadrupole coupling constants can be computed in the following way:

$$\eta = \frac{\chi_{xx} - \chi_{yy}}{\chi_{zz}}. \quad (4)$$

η itself is a measure of the degree of cylindrical symmetry of the electric field gradient and can range from $0 \leq \eta \leq 1$. 0 corresponds to ideal cylindrical symmetry while 1 corresponds to ideal cylindrical asymmetry, *i.e.*, a flat profile. The two different limiting cases and an intermediate value of 0.2 are illustrated in Fig. 13. A value of 0.2 is unreasonably large for the systems studied here and is only chosen so that the changes in η become visible. In principle, six different η are possible resulting from the mapping permutations. The convention of $|\chi_{xx}| \leq |\chi_{yy}| \leq |\chi_{zz}|$ always results in the smallest possible

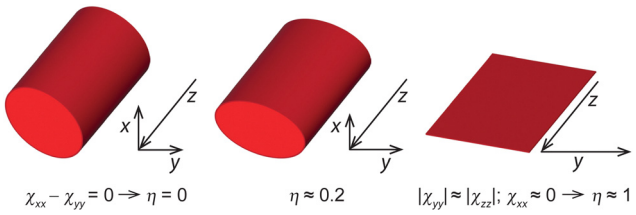

Fig. 13 Illustration of the cylindrical symmetry for values of the asymmetry parameter (η) of 0, 0.2 and 1. The vectors indicate the magnitude of the individual *x*, *y* and *z* components of χ. In case of $\eta \approx 1$, it follows from $|\chi_{yy}| \approx |\chi_{zz}|$ that $\chi_{xx} \approx 0$ due to the tracelessness.

positive η. Typical values range from 0 (very symmetric environments *e.g.* $CClH_3$[101–104]) to around 0.07. The *z* axis can be approximately thought of as the C–Cl/C–Br bond axis with the Cl/Br nucleus as the origin. Another interesting way of visualising χ was proposed by Rinald and Wu.[105] Here, ellipsoids are used derived from a modified Townes–Dailey[106] model.

As was previously mentioned, η is 0 in case of very symmetric species such as *tert*-butyl chloride,[117] $CClH_3$[101–104] or the even simpler HCl,[118] which also holds true for the bromine and iodine analogues. Less symmetric cases such as 2-bromopropane start deviating from this ideal cylindrical case with values around 0.014.[111] If now an OH-group were to be introduced in the 1 position it would be expected that, should a hydrogen bond/contact be formed with the bromine, η should significantly increase. While χ_{zz} remains fairly unchanged since the C–Br bond is not that strongly impacted, the difference between χ_{xx} and χ_{yy} will increase due to polarisation from the hydrogen bond resulting in an increase of η. It should be kept in mind that this relation may not hold for other hydrogen bond arrangements and is specific to the strained intramolecular hydrogen bond arrangement found here. For instance, in case of the water dimer, an increase of η would be expected for the deuterium atom involved in the hydrogen bond relative to the free monomer. However, this change is due to a decrease of χ_{zz}, while χ_{xx} and χ_{yy} remain fairly unchanged. Hence, in either case η may also provide information about the binding geometry.

A variety of halogenated propanes and their η are compared with the propanols studied here in Table 4. In fact, 2-X-propane can be used as a reference system for the 2-gG′ and 2-g′G conformers, while *trans*-1-X-propane can be used for 1-gG′ and *gauche*-1-X-propane for 1-g′G (X = Cl, Br, I). As can be seen, η more than doubles in all cases going from the propane to the propanol case. Hence, η is highly sensitive with regards to the formation of a hydrogen bond. Moreover, the data for the iodopropanes is also shown and very similar to the values found for bromine. Chlorine deviates more strongly, which can be attributed to the rather large experimental uncertainties. In cases where the uncertainties are small, such as 1-gG′, good agreement can be found with the bromine case. Therefore, η for one halogen can be transferred rather well to one another for analogous structures. Computations at the coupled cluster level for the chlorine and bromine containing systems can also be found in the ESI† (Table S11), which are mostly in line with the experimental results.

Considering the sensitivity of η with regards to hydrogen bonding, one might ask if it can be related to the strength of a hydrogen bond itself. To answer this question, we compare η to the corresponding OH-stretching frequencies, which are commonly used to gauge the strength of hydrogen bonds. In general, the lower an OH stretching frequency is the stronger the hydrogen bond, and this shift in frequency is part of the definition of a hydrogen bond itself.[119] Judging from the determined η, it would be expected that 1-g′G (η (^{79}Br) = 0.058 43(95)) has a significantly stronger hydrogen bond than 1-gG′

Table 4 Overview of different values for the asymmetry parameter η for *trans*-1-X-propane, *gauche*-X-propane, 1-X-propanol (1-gG′ and 1-g′G), 2-X-propane and 2-X-propanol (2-gG′ and 2-g′G) with X being ^{35}Cl, ^{37}Cl, ^{79}Br, ^{81}Br, ^{127}I. OH stretching frequencies for the chloro- ($\tilde{\nu}_{Cl}$(OH)) and bromopropanols ($\tilde{\nu}_{Br}$(OH)) are given in cm^{-1}. Here, the revised values for the chloropropanols are shown. Goldstein *et al.*[10] obtained 0.08(15), 0.056(88), 0.0467(92), 0.040(19) and 0.090(60) for 2-gG′ (^{35}Cl), 2-g′G (^{35}Cl), 1-gG′ (^{35}Cl), 1-gG′ (^{37}Cl) and 1-g′G (^{35}Cl), respectively (uncertainties have been calculated by us). Halogen isotope effects upon the OH stretching frequencies are insignificant given the resolution of the Raman setup. Ref. 107 only provides results for χ_{xx}, χ_{yy} and χ_{zz}

	^{35}Cl	^{37}Cl	^{79}Br	^{81}Br	^{127}I	$\tilde{\nu}_{Cl}$(OH)	$\tilde{\nu}_{Br}$(OH)
t-1-X-propane	0.009 4(16)[108]	0.020(21)[108]	0.011 1(12)[107]	0.012 5(16)[107]	0.007 5(5)[109,110]	—	—
g-1-X-propane	0.078(70)[108]	0.043(122)[108]	0.025 6(94)[b]	0.025(13)[b]	0.023 6(25)[109,110]	—	—
1-gG′	0.046 8(37)	0.040 6(90)	0.048 280(66)	0.048 30(10)	—	3619	3608
1-g′G	0.048(16)[c]	0.051(19)[c]	0.060 0(39)[c]	0.061 8(43)[c]	—	3609	3598
2-X-propane	0.013 4(72)[a]	0.013 2(82)[a]	0.014 46(15)[111]	0.014 16(20)[111]	0.015 0(12)[111,112]	—	—
2-gG′	0.039 2(85)[c]	0.029 4(64)[c]	0.039 25(42)	0.039 21(33)	—	3620	3607
2-g′G	0.052(15)	—	0.044 15(24)	0.044 30(37)	—	3620	3608

[a] Derived from the experimental diagonal elements of Meyer *et al.*[113] and χ_{ac} computed by W. C. Bailey ($\chi_{ab} = \chi_{bc} = 0$ MHz).[114] In case of χ_{ac}, an uncertainty of 0.88 MHz and 0.98 MHz (doubling the fitting error of Bailey's method) are assumed for ^{35}Cl and ^{37}Cl, respectively. [b] Derived from the experimental diagonal elements and χ_{ab} of Niide *et al.*[115] and χ_{ac} as well as χ_{bc} computed by W. C. Bailey.[116] In case of χ_{ac} and χ_{bc}, uncertainties were estimated based on doubling Bailey's fitting errors (^{79}Br: 3.16 MHz, ^{81}Br: 2.76 MHz). [c] CCSD(T)-D/awCTZ values were used for components that could not be accurately determined. Uncertainties are based on a and b. We expect that coupled cluster is more accurate than Bailey's method.[98]

(η (^{79}Br) = 0.048 280(66)), since η is considerably larger for the former. For 2-gG′ and 2-g′G, the differences are fairly small and somewhat similar strengths would be expected. In fact, the described behaviour can be found where 1-g′G has a lower OH-stretching frequency by 11 cm^{-1} than 1-gG′. In case of 2-gG′ and 2-g′G, the OH stretching frequencies overlap being in line with similar values for η. Hence, η can in this case be used as a rough measurement for the strength of the hydrogen bond. The corresponding iodopropanols would provide other interesting test cases to see if the observed trends persist. An extension of this analysis to diols is also of interest due to the increase in conformational flexibility allowing for more data points to be included in the analysis. η could also be used as an indicator for the formation of a halogen bond. Here, the halogen atom would have a bridging role instead of a peripheral function. It may be the case that individual χ components are more instructive to judge halogen bonding. However, in terms of theoretical predictions using η may be advantageous due to error compensation, which is briefly discussed in Fig. S5 of the ESI.† Of all tested methods, CCSD(T)/awCTZ by far yields the best predictions for η. In principle, deuterium could also be studied in case of hydrogen bonding as the bridging partner but the low natural abundance, small nuclear quadrupole moment (Q = 0.00286 barn)[90] and limited electric field gradient makes this endeavour experimentally challenging.

4 Summary and conclusions

For all four halogenated chiral (*R*)-propanols, computations predict the gG′ conformer to be more stable than g′G. This chirality induction is consistently larger for 1-ols than for 2-ols (except for BP86/maTZ), and larger for Cl than for Br. Overall, the predictions are fairly consistent with the notable exception of a particularly small coupled cluster chirality induction for 2-bromopropanol. If one considers the CCSD(T) results to be generally correct, DFT underestimates the energetic separation between 1- and 2-ols as well as the separation between Br and Cl alcohols. The described observations also hold true for the MP2 results of Goldstein *et al.*[10]

Coming back to the intramolecular chirality induction[3] issue raised in the introduction, the present work has established in detail which computational methods are best suited, for these systems, to simultaneously describe the three contacts minimally required for any chirality propagation in three-dimensional space: through-bond interaction between the chiral centre and the attached methylene group is tested *via* the correct prediction of rotational constants. The intramolecular hydrogen bond is triply constrained by experimental rotational constants, quadrupole coupling tensor asymmetry, and vibrational shifts. The more subtle through-space interaction of the chirality-defining H/CH$_3$-configuration with the torsional variants of the OH$\cdots$X motif on the opposite side of the chiral centre is again probed by both rotational and vibrational spectroscopy, because a switch between H and CH$_3$ interchanges the two observed conformations of each species. While none of these three interactions is limited to chirality recognition phenomena, their interplay defines the energetical sequence of the resulting transient g′G and gG′ diastereomers for a given enantiomer. Our spectroscopic work thus identifies the most adequate electronic structure methods for future comparative energy decomposition analyses of the involved constitutional, configurational, and conformational isomers. Only a method which correctly describes the structure, dynamics, and electrical field gradients of these chiral model systems can be expected to provide a reliable quantitative description of the chirality induction at play.

The Raman spectra of the chloropropanols and bromopropanols are consistent with the conformational energy predictions. They are quite similar, with the Br spectra being consistently downshifted. Uncertainty due to spectral overlap was removed by microwave spectroscopy. Conformational frequency shifts are described very well by harmonic coupled cluster theory. For some systems, the (*meta*)-GGAs and also MP2 significantly underestimate the harmonic shifts. For others, MP2 performs well, including the MP2/6-311++G(d,p) results of Goldstein *et al.* for the chloropropanols.[10] The hybrid and double hybrid functionals perform more systematically, with CAM-B3LYP yielding the best results among them. Anharmonic correction consistently improves the results. Switching from the aTZ to the significantly faster maTZ basis set has negligible effects on both the relative zero point corrected energies (see also ref. 56) as well as the harmonic frequency shifts. We thus recommend the use of maTZ.

In terms of absolute predictions for the OH-stretching wavenumbers, harmonic BP86 is fortuitously close to the experiment, but like PBE and TPSS rather inconsistent across systems. After anharmonic VPT2 correction, most methods predict fundamental wavenumbers that are too small, whereas PBE0 and CAM-B3LYP overestimate experiment. The deviations from experiment found for CAM-B3LYP and especially B2PLYP are very consistent across different systems. In fact, by adding 13 cm^{-1} to the B2PLYP results (and to a lesser extent by subtracting 28 cm^{-1} for CAM-B3LYP) good predictions for fundamental wavenumbers can be obtained. It remains to be seen if such an empirical correction is also applicable to similar systems.

For the predictions of *A*, *B* and *C*, it is noticeable that the maximum deviations are generally smaller for the bromopropanols than for the Cl analogues. However, the median of the deviations remains remarkably similar between the halogenated alcohols for the results based on equilibrium geometries. The small spread and consistency of BP86 and PBE invites low cost predictions after empirical correction. Equilibrium geometry B3LYP predicts *A* very well but the vibrationally averaged VPT2 results reveal the error compensation involved. In contrast, PBE0 consistently improves with the VPT2 correction. Therefore, it can be argued that the equilibrium predictions of B3LYP are right for the wrong reason, while the opposite is true for PBE0. For the same reason, equilibrium structure coupled cluster results significantly overestimate *A* for the bromopropanols. For *B* and *C*, these vibrational effects are much smaller

in absolute terms, explaining the good performance of equilibrium structure CCSD(T).

For the predictions of the quartic centrifugal distortion constants, all tested methods are generally able to reproduce the right order of magnitude and sign, which already can be of great help where experimental assignments prove to be difficult. Furthermore, most methods are able to reproduce D_J, d_1 and d_2 quite well. D_K and D_{JK} appear to be harder to predict. A recent study of Franke and Stanton[95] suggests that this may be related to the fact that no vibrational corrections are included to the distortion constants in VPT2. Their partial VPT4 calculations for methanediol show that D_K and D_{JK} are impacted the most. Among the methods tested here, B2PLYP and CAM-B3LYP perform the best. Distortion constants at the coupled cluster level do not provide an advantage, although this may be related to the lack of vibrational effects in VPT2. Moreover, for d_1 and d_2 a significant outlier can be observed for the g′G conformer of 1-chlorpropan-2-ol. Given that all methods predict similar values and that the Br analogue shows no such behaviour, it may be the case that theory is more reliable than experiment in this instance without additional transitions. Although a value of −0.127(21) kHz, for d_1 for instance, may seem converged judging by the uncertainty, it should be kept in mind that this uncertainty is correlated with others and does not necessarily indicate convergence towards the actual experimental value.

The computational results for the nuclear quadrupole coupling constants χ_{ij} are inconsistent between the chloro- and bromopropanols due to the much larger quadrupole moment of Br. For the bromopropanols, χ_{aa} is consistently underestimated with the exception of relativistic CCSD(T), while for χ_{bb-cc} most methods centre around 0 MHz, with a considerable spread except for relativistic CCSD(T). This may be related to 1-gG′ (where Br lies within the C–C–C backbone plane) not being accurately described in many instances. Overall, relativistic CCSD(T) performs best and manages to reduce the spread of the deviations in comparison to the non-relativistic variant. BP86, PBE, and to a lesser extent B3LYP/maTZ yield good results with fairly small spreads. Hence, an empirical correction might be possible for other Br compounds.

For chloropropanols, experimental accuracy becomes limiting in several cases. Coupled cluster appears to perform well, expectedly independent of relativistic effects. BP86 and PBE can again be used as a cost-effective alternative. The seemingly good performance of the GGAs may be related to error compensation from projection of the electric field gradient to the inertial principal axis system.[98]

Considering all properties studied in this work, only CCSD(T) is seen to perform consistently well after estimating anharmonic and relativistic effects, confirming its ''gold standard'' reputation. Harmonic B3LYP has a favourable price-performance ratio, but we demonstrate several cases of fortuitous error cancellation.

Lastly, we address the potential of the asymmetry parameter η of the nuclear quadrupole coupling tensor as a probe for the hydrogen bond strength and geometry. For the systems studied here, η generally increases when the corresponding OH stretching wavenumber decreases, indicative of an increasing hydrogen bond strength. This is related to an increasing anisotropy orthogonal to the C–X bond, if the hydrogen bond is not collinear with C–X. The comparison between propane and propanol derivatives underscores the sensitivity of η to hydrogen bonding. It would be interesting to extend this analysis to iodine, to the conformationally more diverse diols and finally to halogen bonding, where X (X = Cl, Br, I) is involved even more directly.

Author contributions

Conceptualisation: BH; data curation: BH, MS, DAO; formal analysis: BH, DAO; funding acquisition: MAS, MS, DAO; investigation: BH; supervision: MAS, MS, DAO; visualisation: BH; writing – original draft: BH; writing – review & editing: BH, MS, MAS, DAO.

Conflicts of interest

The authors have no conflicts of interest to declare.

Acknowledgements

Parts of this work have previously been published in the PhD thesis of Beppo Hartwig.[120] This work was funded by the Deutsche Forschungsgemeinschaft (DFG, German Research Foundation) – 389479699/GRK2455, OB 535/1-1, and 405832858 for computational resources. We greatly thank Dr Arman Nejad for the computation of the centrifugal distortion constants at the coupled cluster level.

Notes and references

1 M. M. Green, M. P. Reidy, R. D. Johnson, G. Darling, D. J. O'Leary and G. Willson, *J. Am. Chem. Soc.*, 1989, **111**, 6452–6454.
2 C. Wolf, *Dynamic Stereochemistry of Chiral Compounds*, The Royal Society of Chemistry, 2007.
3 A. Zehnacker and M. A. Suhm, *Angew. Chem., Int. Ed.*, 2008, **47**, 6970–6992.
4 R. B. Sunoj, *Acc. Chem. Res.*, 2016, **49**, 1019–1028.
5 N. Borho and Y. Xu, *Angew. Chem., Int. Ed.*, 2007, **46**, 2276–2279.
6 J. Thomas, W. Jäger and Y. Xu, *Angew. Chem., Int. Ed.*, 2014, **53**, 7277–7280.
7 M. Lange, E. Sennert and M. A. Suhm, *Symmetry*, 2022, **14**, 357.
8 V. R. Meyer and M. Rais, *Chirality*, 1989, **1**, 167–169.
9 A. Al-Rabaa, E. Bréhéret, F. Lahmani and A. Zehnacker, *Chem. Phys. Lett.*, 1995, **237**, 480–484.
10 T. Goldstein, M. Snow and B. Howard, *J. Mol. Spectrosc.*, 2006, **236**, 1–10.

11 M. Heger, K. E. Otto, R. A. Mata and M. A. Suhm, *Phys. Chem. Chem. Phys.*, 2015, **17**, 9899–9909.
12 A. N. Mort and Y. Xu, *J. Mol. Spectrosc.*, 2023, **392**, 111745.
13 N. O. B. Lüttschwager and M. A. Suhm, *Soft Matter*, 2014, **10**, 4885–4901.
14 T. Forsting, H. C. Gottschalk, B. Hartwig, M. Mons and M. A. Suhm, *Phys. Chem. Chem. Phys.*, 2017, **19**, 10727–10737.
15 M. Gawrilow and M. A. Suhm, *Molecules*, 2021, **26**, 4523.
16 B. Hartwig, *Göttingen Research Online/Data*, 2022, version V1, DOI: **10.25625/EJVBHD**.
17 H. Schaal, T. Häber and M. A. Suhm, *J. Phys. Chem. A*, 2000, **104**, 265–274.
18 J. Durig, S. Shen and G. Guirgis, *J. Mol. Struct.*, 2001, **560**, 295–314.
19 T. Scharge, T. N. Wassermann and M. A. Suhm, *Z. Phys. Chem.*, 2008, **222**, 1407–1452.
20 T. N. Wassermann and M. A. Suhm, *J. Phys. Chem. A*, 2010, **114**, 8223–8233.
21 T. N. Wassermann, M. A. Suhm, P. Roubin and S. Coussan, *J. Mol. Struct.*, 2012, **1025**, 20–32.
22 K. E. Otto, Z. Xue, P. Zielke and M. A. Suhm, *Phys. Chem. Chem. Phys.*, 2014, **16**, 9849–9858.
23 D. Schmitz, V. A. Shubert, T. Betz and M. Schnell, *J. Mol. Spectrosc.*, 2012, **280**, 77–84.
24 C. Pérez, A. Krin, A. L. Steber, J. C. López, Z. Kisiel and M. Schnell, *J. Phys. Chem. Lett.*, 2016, **7**, 154–160.
25 U. Andresen, H. Dreizler, U. Kretschmer, W. Stahl and C. Thomsen, *Fresenius' J. Anal. Chem.*, 1994, **349**, 272–276.
26 T. J. Balle and W. H. Flygare, *Rev. Sci. Instrum.*, 1981, **52**, 33–45.
27 M. Schnell, D. Banser and J. U. Grabow, *Rev. Sci. Instrum.*, 2004, **75**, 2111–2115.
28 H. M. Pickett, *J. Mol. Spectrosc.*, 1991, **148**, 371–377.
29 F. Neese, *Wiley Interdiscip. Rev.: Comput. Mol. Sci.*, 2012, **2**, 73–78.
30 F. Neese, *Wiley Interdiscip. Rev.: Comput. Mol. Sci.*, 2017, **8**, e1327.
31 F. Neese, F. Wennmohs, U. Becker and C. Riplinger, *J. Chem. Phys.*, 2020, **152**, 224108.
32 M. J. Frisch, G. W. Trucks, H. B. Schlegel, G. E. Scuseria, M. A. Robb, J. R. Cheeseman, G. Scalmani, V. Barone, G. A. Petersson, H. Nakatsuji, X. Li, M. Caricato, A. V. Marenich, J. Bloino, B. G. Janesko, R. Gomperts, B. Mennucci, H. P. Hratchian, J. V. Ortiz, A. F. Izmaylov, J. L. Sonnenberg, D. Williams-Young, F. Ding, F. Lipparini, F. Egidi, J. Goings, B. Peng, A. Petrone, T. Henderson, D. Ranasinghe, V. G. Zakrzewski, J. Gao, N. Rega, G. Zheng, W. Liang, M. Hada, M. Ehara, K. Toyota, R. Fukuda, J. Hasegawa, M. Ishida, T. Nakajima, Y. Honda, O. Kitao, H. Nakai, T. Vreven, K. Throssell, J. A. Montgomery, Jr., J. E. Peralta, F. Ogliaro, M. J. Bearpark, J. J. Heyd, E. N. Brothers, K. N. Kudin, V. N. Staroverov, T. A. Keith, R. Kobayashi, J. Normand, K. Raghavachari, A. P. Rendell, J. C. Burant, S. S. Iyengar, J. Tomasi, M. Cossi, J. M. Millam, M. Klene, C. Adamo, R. Cammi, J. W. Ochterski, R. L. Martin, K. Morokuma, O. Farkas, J. B. Foresman and D. J. Fox, *Gaussian 16 Revision A.03*, Gaussian Inc., Wallingford CT, 2016.
33 H.-J. Werner, P. J. Knowles, G. Knizia, F. R. Manby and M. Schütz, *Wiley Interdiscip. Rev.: Comput. Mol. Sci.*, 2012, **2**, 242–253.
34 H.-J. Werner, P. J. Knowles, F. R. Manby, J. A. Black, K. Doll, A. Heßelmann, D. Kats, A. Köhn, T. Korona, D. A. Kreplin, Q. Ma, T. F. Miller, A. Mitrushchenkov, K. A. Peterson, I. Polyak, G. Rauhut and M. Sibaev, *J. Chem. Phys.*, 2020, **152**, 144107.
35 H.-J. Werner, P. J. Knowles, G. Knizia, F. R. Manby, M. Schütz, P. Celani, W. Györffy, D. Kats, T. Korona, R. Lindh, A. Mitrushenkov, G. Rauhut, K. R. Shamasundar, T. B. Adler, R. D. Amos, S. J. Bennie, A. Bernhardsson, A. Berning, D. L. Cooper, M. J. O. Deegan, A. J. Dobbyn, F. Eckert, E. Goll, C. Hampel, A. Hesselmann, G. Hetzer, T. Hrenar, G. Jansen, C. Köppl, S. J. R. Lee, Y. Liu, A. W. Lloyd, Q. Ma, R. A. Mata, A. J. May, S. J. McNicholas, W. Meyer, T. F. Miller III, M. E. Mura, A. Nicklass, D. P. ONeill, P. Palmieri, D. Peng, T. Petrenko, K. Pflüger, R. Pitzer, M. Reiher, T. Shiozaki, H. Stoll, A. J. Stone, R. Tarroni, T. Thorsteinsson, M. Wang and M. Welborn, *MOLPRO, version 2020.2, a package of ab initio programs*, 2020, see **https://www.molpro.net**.
36 J. P. Perdew, *Phys. Rev. B: Condens. Matter Mater. Phys.*, 1986, **33**, 8822–8824.
37 J. P. Perdew, *Phys. Rev. B: Condens. Matter Mater. Phys.*, 1986, **34**, 7406.
38 A. D. Becke, *Phys. Rev. A: At., Mol., Opt. Phys.*, 1988, **38**, 3098–3100.
39 J. P. Perdew, K. Burke and M. Ernzerhof, *Phys. Rev. Lett.*, 1996, **77**, 3865–3868.
40 J. Tao, J. P. Perdew, V. N. Staroverov and G. E. Scuseria, *Phys. Rev. Lett.*, 2003, **91**, 146401.
41 B. Miehlich, A. Savin, H. Stoll and H. Preuss, *Chem. Phys. Lett.*, 1989, **157**, 200–206.
42 C. Lee, W. Yang and R. G. Parr, *Phys. Rev. B: Condens. Matter Mater. Phys.*, 1988, **37**, 785–789.
43 C. Adamo and V. Barone, *J. Chem. Phys.*, 1999, **110**, 6158–6170.
44 M. Ernzerhof and G. E. Scuseria, *J. Chem. Phys.*, 1999, **110**, 5029–5036.
45 H. Iikura, T. Tsuneda, T. Yanai and K. Hirao, *J. Chem. Phys.*, 2001, **115**, 3540–3544.
46 T. Yanai, D. P. Tew and N. C. Handy, *Chem. Phys. Lett.*, 2004, **393**, 51–57.
47 C. Møller and M. S. Plesset, *Phys. Rev.*, 1934, **46**, 618–622.
48 S. Grimme, *J. Chem. Phys.*, 2006, **124**, 034108.
49 T. Schwabe and S. Grimme, *Phys. Chem. Chem. Phys.*, 2007, **9**, 3397–3406.
50 S. Grimme, J. Antony, S. Ehrlich and H. Krieg, *J. Chem. Phys.*, 2010, **132**, 154104.
51 S. Grimme, S. Ehrlich and L. Goerigk, *J. Comput. Chem.*, 2011, **32**, 1456–1465.
52 B. M. Axilrod and E. Teller, *J. Chem. Phys.*, 1943, **11**, 299–300.
53 Y. Muto, *J. Phys. Math. Soc. Jpn.*, 1943, **17**, 629.

54 J. Zheng, X. Xu and D. G. Truhlar, *Theor. Chem. Acc.*, 2011, **128**, 295–305.
55 F. Weigend and R. Ahlrichs, *Phys. Chem. Chem. Phys.*, 2005, **7**, 3297.
56 X. Aniban, B. Hartwig, A. Wuttke and R. A. Mata, *Phys. Chem. Chem. Phys.*, 2021, **23**, 12093–12104.
57 D. Bykov, T. Petrenko, R. Izsák, S. Kossmann, U. Becker, E. Valeev and F. Neese, *Mol. Phys.*, 2015, **113**, 1961–1977.
58 F. Weigend, *Phys. Chem. Chem. Phys.*, 2006, **8**, 1057.
59 B. Hartwig and M. A. Suhm, *Phys. Chem. Chem. Phys.*, 2021, **23**, 21623–21640.
60 H. H. Nielsen, *Rev. Mod. Phys.*, 1951, **23**, 90–136.
61 V. Barone, *J. Chem. Phys.*, 2005, **122**, 014108.
62 V. Barone, J. Bloino, C. A. Guido and F. Lipparini, *Chem. Phys. Lett.*, 2010, **496**, 157–161.
63 T. H. Dunning, *J. Chem. Phys.*, 1989, **90**, 1007–1023.
64 R. A. Kendall, T. H. Dunning and R. J. Harrison, *J. Chem. Phys.*, 1992, **96**, 6796–6806.
65 W. Gordy and R. Cook, *Microwave Molecular Spectra*, Interscience Pub., 1970.
66 J. K. G. Watson, in *Vibrational spectra and structure*, ed. J. R. Durig, Elsevier Scientific Publishing Company, Amsterdam, 1977, vol. 6, pp. 1–89.
67 J. Z. Gong, D. A. Matthews, P. B. Changala and J. F. Stanton, *J. Chem. Phys.*, 2018, **149**, 114102.
68 W. Györffy, G. Knizia and H.-J. Werner, *J. Chem. Phys.*, 2017, **147**, 214101.
69 W. Györffy and H.-J. Werner, *J. Chem. Phys.*, 2018, **148**, 114104.
70 T. B. Adler, G. Knizia and H.-J. Werner, *J. Chem. Phys.*, 2007, **127**, 221106.
71 G. Knizia, T. B. Adler and H.-J. Werner, *J. Chem. Phys.*, 2009, **130**, 054104.
72 K. A. Peterson, T. B. Adler and H.-J. Werner, *J. Chem. Phys.*, 2008, **128**, 84102.
73 J. G. Hill and K. A. Peterson, *J. Chem. Phys.*, 2014, **141**, 094106.
74 K. A. Peterson, D. Figgen, E. Goll, H. Stoll and M. Dolg, *J. Chem. Phys.*, 2003, **119**, 11113–11123.
75 F. Weigend, A. Köhn and C. Hättig, *J. Chem. Phys.*, 2002, **116**, 3175–3183.
76 K. E. Yousaf and K. A. Peterson, *J. Chem. Phys.*, 2008, **129**, 184108.
77 K. E. Yousaf and K. A. Peterson, *Chem. Phys. Lett.*, 2009, **476**, 303–307.
78 F. Weigend, *J. Comput. Chem.*, 2008, **29**, 167–175.
79 K. A. Peterson and T. H. Dunning, *J. Chem. Phys.*, 2002, **117**, 10548–10560.
80 N. J. DeYonker, K. A. Peterson and A. K. Wilson, *J. Phys. Chem. A*, 2007, **111**, 11383–11393.
81 A. Aerts and A. Brown, *J. Chem. Phys.*, 2019, **150**, 224302.
82 S. Stopkowicz, L. Cheng, M. E. Harding, C. Puzzarini and J. Gauss, *Mol. Phys.*, 2013, **111**, 1382–1389.
83 K. Gaul and R. Berger, *Mol. Phys.*, 2020, **118**, e1797199.
84 D. Lv, A. Maris, L. Evangelisti, A. Maggio, W. Song, A. A. Elliott, S. A. Peebles, J. L. Neill, M. T. Muckle, B. H. Pate, R. A. Peebles and S. Melandri, *Phys. Chem. Chem. Phys.*, 2021, **23**, 18093–18101.
85 M. Douglas and N. M. Kroll, *Ann. Phys.*, 1974, **82**, 89–155.
86 B. A. Hess, *Phys. Rev. A: At., Mol., Opt. Phys.*, 1986, **33**, 3742–3748.
87 G. Jansen and B. A. Hess, *Phys. Rev. A: At., Mol., Opt. Phys.*, 1989, **39**, 6016–6017.
88 L. Visscher and K. Dyall, *At. Data Nucl. Data Tables*, 1997, **67**, 207–224.
89 F. Neese, A. Wolf, T. Fleig, M. Reiher and B. A. Hess, *J. Chem. Phys.*, 2005, **122**, 204107.
90 N. Stone, *Table of Nuclear Magnetic Dipole and Electric Quadrupole Moments (INDC(NDS)-0658)*, International Atomic Energy Agency (IAEA), 2014.
91 A. K. King and B. J. Howard, *J. Mol. Spectrosc.*, 2001, **205**, 38–42.
92 A. A. Rabaa, K. Le Barbu, F. Lahmani and A. Zehnacker-Rentien, *J. Phys. Chem. A*, 1997, **101**, 3273–3278.
93 K. M. S. Gonçalves, D. R. Garcia, T. C. Ramalho, J. D. Figueroa-Villar and M. P. Freitas, *J. Phys. Chem. A*, 2013, **117**, 10980–10984.
94 S. Grimme, *Chem. – Eur. J.*, 2012, **18**, 9955–9964.
95 P. R. Franke and J. F. Stanton, *J. Phys. Chem. A*, 2023, **127**, 924–937.
96 B. S. Ray, *Z. Phys.*, 1932, **78**, 74–91.
97 H.-Y. Jian, C.-T. Yang and L.-K. Chu, *Phys. Chem. Chem. Phys.*, 2021, **23**, 14699–14705.
98 R. Dohmen, D. Fedosov and D. A. Obenchain, *Phys. Chem. Chem. Phys.*, 2022, **25**, 2420–2429.
99 R. A. Mata and M. A. Suhm, *Angew. Chem., Int. Ed.*, 2017, **56**, 11011–11018.
100 Z. Kisiel, *QDIAG Version 12.II.2023*, PROSPE-Programs for ROtational SPEctroscopy, 2023.
101 S. G. Kukolich and A. C. Nelson, *J. Am. Chem. Soc.*, 1973, **95**, 680–682.
102 H.-T. Man and R. Butcher, *J. Mol. Spectrosc.*, 1985, **110**, 19–26.
103 G. Wlodarczak, D. Boucher, R. Bocquet and J. Demaison, *J. Mol. Spectrosc.*, 1986, **116**, 251–255.
104 L. Nová Stříteská, M. Šimečková, P. Kania, P. Musil, L. Kolesniková, J. Koubek and Š. Urban, *J. Mol. Struct.*, 2009, **919**, 89–93.
105 A. Rinald and G. Wu, *J. Phys. Chem. A*, 2020, **124**, 1176–1186.
106 C. H. Townes and B. P. Dailey, *J. Phys. Chem.*, 1949, **17**, 782–796.
107 E. A. Arsenault, D. A. Obenchain, T. A. Blake, S. Cooke and S. E. Novick, *J. Mol. Spectrosc.*, 2017, **335**, 17–22.
108 A. de Luis, M. Sanz, F. J. Lorenzo, J. C. López and J. L. Alonso, *J. Mol. Spectrosc.*, 1997, **184**, 60–77.
109 Y. Niide, I. Ohkoshi and M. Takano, *J. Mol. Spectrosc.*, 1987, **122**, 113–129.
110 M. Fujitake and M. Hayashi, *J. Mol. Spectrosc.*, 1988, **127**, 112–124.
111 C. Ikeda, T. Inagusa and M. Hayashi, *J. Mol. Spectrosc.*, 1989, **135**, 334–348.

112 J. Gripp and H. Dreizler, *Zeitschrift für Naturforschung A*, 1990, **45**, 715–723.
113 M. Meyer, J.-U. Grabow, H. Dreizler and H. D. Rudolph, *J. Mol. Spectrosc.*, 1992, **151**, 217–242.
114 W. C. Bailey, *Calculation of Nuclear Quadrupole Coupling Constants in Gaseous State Molecules; 2-Chloropropane*, **https://nqcc.wcbailey.net/CH32CHCl.html**, last visited on 23.04.2023.
115 Y. Niide, I. Ohkoshi and M. Takano, *J. Mol. Spectrosc.*, 1981, **89**, 387–396.
116 W. C. Bailey, Calculation of Nuclear Quadrupole Coupling Constants in Gaseous State Molecules; 2-Chloropropane, **https://nqcc.wcbailey.net/Propanes.pdf**, last visited on 23.04.2023.
117 Z. Kisiel, E. Białkowska-Jaworska, O. Desyatnyk, B. Pietrewicz and L. Pszczółkowski, *J. Mol. Spectrosc.*, 2001, **208**, 113–120.
118 T. Klaus, S. Belov and G. Winnewisser, *J. Mol. Spectrosc.*, 1998, **187**, 109–117.
119 E. Arunan, G. R. Desiraju, R. A. Klein, J. Sadlej, S. Scheiner, I. Alkorta, D. C. Clary, R. H. Crabtree, J. J. Dannenberg, P. Hobza, H. G. Kjaergaard, A. C. Legon, B. Mennucci and D. J. Nesbitt, *Pure Appl. Chem.*, 2011, **83**, 1637–1641.
120 B. Hartwig, PhD thesis, Georg-August-Universität Göttingen, Germany, 2022, DOI: **10.53846/goediss-9628**.

